nuclear fusion
IAEA

PAPER • OPEN ACCESS

Predictive integrated modelling of the hybrid and baseline scenarios of JT-60SA in view of the second operational phase

To cite this article: S. Gabriellini *et al* 2025 *Nucl. Fusion* **65** 056041

View the article online for updates and enhancements.

You may also like

- Analysis of JT-60SA operational scenarios
L. Garzotti, E. Barbato, J. Garcia et al.
- L-mode plasmas analyses and current ramp-up predictions for a JT-60SA hybrid scenario
J Morales, J Garcia, G Giruzzi et al.
- Generalization of a fast, predictive model for tokamak scenario design in ASTRA and comparison to a RAPTOR model
Raphael Schramm, Alexander Bock, Emiliano Fable et al.

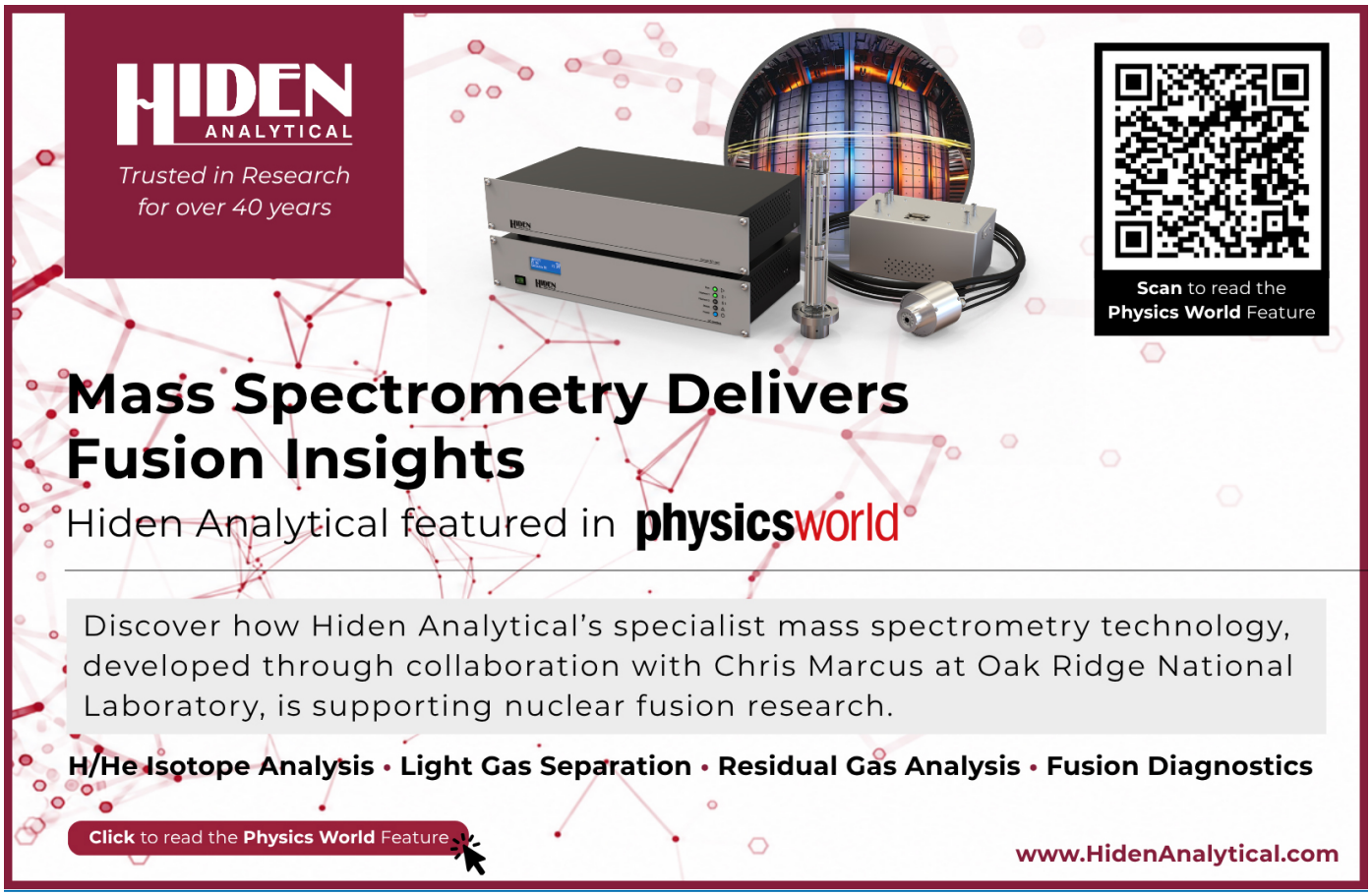

This content was downloaded from IP address 81.57.8.77 on 03/09/2026 at 10:46

OPEN ACCESS
IOP Publishing | International Atomic Energy Agency
Nuclear Fusion
Nucl. Fusion **65** (2025) 056041 (21pp)
https://doi.org/10.1088/1741-4326/adcb4f

Predictive integrated modelling of the hybrid and baseline scenarios of JT-60SA in view of the second operational phase

S. Gabriellini[1], V.K. Zotta[1,*], L. Garzotti[2], N. Aiba[3], J.-F. Artaud[4], G. Giruzzi[4], G. Pucella[5], C. Sozzi[6], D. Taylor[2], T. Wakatsuki[3], L. Burla[1], C. Leoni[1], R. Gatto[1] and the JT-60SA integrated project team[a]

[1] Dipartimento di Ingegneria Astronautica, Elettrica ed Energetica, Sapienza Università di Roma, Via Eudossiana 18, 00184 Roma, Italy
[2] UK Atomic Energy Authority (UKAEA), Culham Campus, Abingdon, United Kingdom of Great Britain and Northern Ireland
[3] National Institutes for Quantum Science and Technology, Naka 311-0193, Japan
[4] CEA, IRFM, F-13108 Saint Paul Lez Durance, France
[5] ENEA C. R. Frascati, Frascati, Italy
[6] ISTP Istituto di Scienza e Tecnologia del Plasma—CNR, Milano, Italy

E-mail: vitokonrad.zotta@uniroma1.it

Received 11 January 2025, revised 18 March 2025
Accepted for publication 10 April 2025
Published 28 April 2025

Abstract

The integrated modelling of two plasma scenarios, hybrid and baseline, envisaged for the second operational phase (OP2) of the JT-60SA tokamak has been performed using the 1.5-dimensional JINTRAC suite of codes and the Bohm/gyro-Bohm (BgB) semi-empirical transport model. The decision to use the BgB model is driven not only by its widespread application in predicting scenarios for JET and JT-60U similar to those anticipated for JT-60SA, but also by its low computational cost. Two versions of the hybrid scenario—3.7 MA/2.28 T and 2.7 MA/1.70 T with $P_{aux} = 19$ MW—were optimized with respect to the reference METIS simulation to maintain a safety factor with a low magnetic shear region, $q_{min} > 1$ and low shine-through losses. The results suggest that a high-β_N ($\sim$3) regime with a high non-inductive current fraction ($\sim$70%) could be achieved during the initial research phase at 2.7 MA/1.70 T and at a Greenwald density fraction $n_e/n_{GW} = 0.4$. Hybrid-like q profiles are expected to be more easily obtained at higher Greenwald density fractions (0.6–0.8), while at lower densities, challenges such as hollow current density profiles and reversed q profiles were mitigated by adjusting the negative-neutral beam injection power and the injector configuration. The baseline scenario—4.6 MA/2.28 T with $P_{aux} = 17.5$ MW—demonstrated potential for high confinement

[a] See Shirai *et al* 2024 (https://doi.org/10.1088/1741-4326/ad34e4) for the JT-60SA integrated project team.
[*] Author to whom any correspondence should be addressed.

Original Content from this work may be used under the terms of the Creative Commons Attribution 4.0 licence. Any further distribution of this work must maintain attribution to the author(s) and the title of the work, journal citation and DOI.

 © 2025 The Author(s). Published by IOP Publishing Ltd on behalf of the IAEA

performance, achieving values of $\beta_N \sim 1.8$, $H_{98} \sim 1.0$, and $W_{th} \sim 10$ MJ. A scan of the temperature pedestal height and its effect on plasma performance underscores the need to develop a physics-based model capable of accurately predicting the H-mode pedestal.

Keywords: nuclear fusion, magnetic confinement, tokamak, JT-60SA, plasma simulations

(Some figures may appear in colour only in the online journal)

1. Introduction

JT-60SA, currently the largest superconducting tokamak in the world, is a fusion experiment jointly constructed and operated by Europe and Japan, aimed at supporting the development of ITER and addressing key physics and engineering challenges for future demonstration power plants [1, 2].

The machine successfully produced its first plasma in October 2023, following the completion of the Integrated Commissioning phase (IC), and concluded its first operational phase (OP1) in December 2023 [3, 4]. During this initial phase, plasma control schemes were tested [5], and the machine's basic performance was assessed by progressively increasing the plasma current and discharge duration, initially in a limiter configuration, followed by an open upper divertor configuration [4]. A plasma current of 1 MA at a toroidal magnetic field of 2 T was sustained for several seconds using both He and H as main ion species, with a maximum electron cyclotron resonance heating (ECRH) power of 1.5 MW. The formation of strike points was confirmed through EDICAM video diagnostics [7], and preliminary estimates of the energy confinement time ($\tau_E \sim$100–200 ms) were found to be consistent with the ITER89-P scaling laws [6]. Additionally, the experimental data obtained during IC/OP1 is being used to validate equilibrium control codes [8] and to establish a disruption database to ensure the safety of future plasma operations [9].

The experience gained from the successful start-up of a large superconducting tokamak like JT-60SA will be useful in mitigating the risks associated with future ITER operations.

The high flexibility of the JT-60SA tokamak allows for the study of a wide variety of scenarios, particularly:

- pulsed, inductive baseline scenarios;
- advanced inductive, high-beta, low magnetic shear hybrid scenarios;
- fully non-inductive, steady-state advanced scenarios.

The 0-dimensional (0-D) parameters of these scenarios, detailed in tables 1-3 and 3-1 of [1], were initially determined using the 2D free-boundary equilibrium code ACCOME [13]. These parameters were subsequently validated and systematically refined using the 0.5-D METIS code [14]. The METIS results show strong agreement with those from ACCOME, as reported in [15], and serve as a foundation for more advanced 1.5-D transport simulations.

The 1.5-D transport simulations were performed for the flat-top phase of the main JT-60SA operational scenarios using various integrated modelling suites of codes (JINTRAC [16], ASTRA [17], CRONOS [18], TOPICS [19]) and different transport models (GLF23 [20], CDBM [21], and Bohm/gyro-Bohm (BgB) [22]), as extensively detailed in [23]. These simulations indicate that the predictions for the flat-top phase align well with the projected scenarios, with discrepancies in key 0-D plasma parameters between the codes being between 30% and 40%—if the properties of the H-mode pedestals are similar—even though local differences in kinetic profiles can be significant (up to 70%).

These integrated modelling suites of codes have been widely employed at JET for predicting fusion power in the DTE2 experimental campaign [24–26], as well as for informing experiments on the optimal fuelling scheme to achieve a 50-50 D-T mixture [27], further demonstrating their effectiveness in supporting the development of plasma scenarios.

Moreover, to determine whether the projected plasma parameters for the flat-top phase can be realistically achieved, and under which assumptions, it is essential to model the ramp-up phase as well. A staged approach is typically adopted for this.

First, an initial estimate of the plasma shape evolution is obtained with equilibrium codes, such as MECS [28, 29]. Then, the ramp-up phase is designed using a fast simulator, such as METIS, based on the initial estimate of the plasma shape evolution. The necessary currents in the poloidal field coils to achieve this shape are calculated using a free-boundary equilibrium code in inverse mode, such as FEEQS [30]. By iterating between METIS and FEEQS, with continuous updates to the plasma boundary, it is possible to verify whether poloidal field coil currents, terminal voltages, maximum forces, and magnetic field limits remain within machine constraints, thereby ensuring the feasibility of the scenario [31]. Once feasibility is confirmed, the controllability of the scenario is assessed using equilibrium control codes, such as CREATE-NL [33] and MECS.

Moreover, recent efforts have focused on the numerical optimisation of the waveforms of actuators during the ramp-up phase [34–36], aiming to satisfy the scenario constraints by minimising a given cost function. Additionally, a numerical optimisation has been applied to the ITER hybrid scenario [37].

After confirming feasibility and control, the ramp-up phase can be further verified and refined using more sophisticated integrated modelling codes, allowing for additional scenario optimization. This approach has been extensively applied in

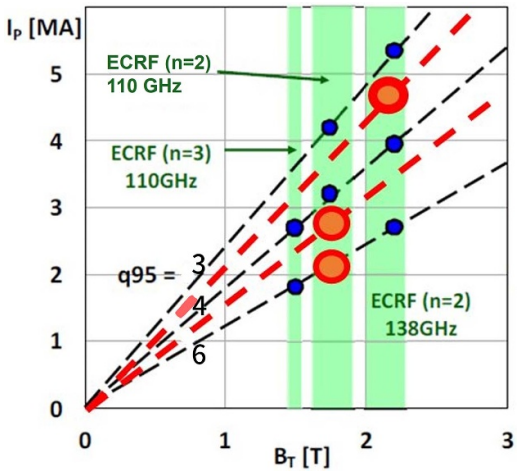

Figure 1. Range of plasma current (I_p) and magnetic field (B_t) for the JT-60SA operational scenarios planned for the initial research phase with ECRF heating. Scenarios anticipated for Operation Phase 2 (OP2) are indicated with red circles. Reproduced with permission from JT-60SA [1].

the modelling and optimization of ITER operational scenarios [38–40]. On JT-60SA, this method was tested for the ramp-up phase of the advanced inductive (hybrid) scenario [41] and subsequently extended to provide preliminary predictions for the baseline and hybrid scenarios envisaged for the second operational phase (OP2), as detailed in [42].

The work presented in this paper builds upon the preliminary study reported in [41, 42], with the goal of extending the modelling of [42] to different combinations of plasma current, toroidal magnetic field, and density, while optimizing the scenarios in preparation for the upcoming second operational phase of JT-60SA.

Three scenarios are being developed for OP2, as indicated by the red circles in figure 1:

- $q_{95} \sim 3$ scenario (OP2 baseline operation): 4.6 MA/2.28 T ($q_{95} \sim 3.0$), $n_e \sim 4.5$–6.7×10^{19} m^{-3} ($f_{gw} \sim 0.4$–0.6), $P_{NB} = 16$ MW, $P_{EC} = 1.5$ MW, $\beta_N \sim 2.0$, $H_H \sim 1$.
- $q_{95} \sim 4$ scenario (OP2 hybrid operation): 2.7 MA/1.70 T ($q_{95} \sim 4.0$), $n_e > 2.7 \times 10^{19}$ m^{-3} ($f_{gw} > 0.4$), $P_{NB} = 16$ MW, $P_{EC} = 3$ MW, $\beta_N \sim 2$–3, $H_H > 1.1$.
- $q_{95} > 6$ scenario (OP2 ITB operation): 1.7–2.0 MA/1.70 T ($q_{95} > 6.0$), $n_e > 2$–2.5×10^{19} m^{-3} ($f_{gw} > 0.5$), $P_{NB} = 16$ MW, $P_{EC} = 3$ MW, $\beta_N > 3.5$, $H_H > 1.2$.

In this initial phase the auxiliary heating power will be limited. The available neutral beam injection (NBI) power will be 23.5 MW (in deuterium) while the available ECRH will be 3 MW, both of which exceed the capacities installed during OP1, though still less than what will be available for the Extended Research Phase [1]. Additionally, the tokamak will be equipped with an inertially cooled carbon divertor and a divertor cryopump, capable of withstanding a heat flux of 10 MW m^{-2} for 7.5 s and 15 MW m^{-2} for 5 s [10–12].

This paper presents the JINTRAC integrated modelling of the ramp-up phase for the OP2 hybrid and baseline scenarios, while the modelling of the OP2 ITB operation will be presented in future work. The simulations of this paper serve as a starting point for future physics studies and optimizations.

The paper is organized as follows: In section 2, the models used to simulate the scenarios are described. Section 3 presents the results of the modelling for the hybrid scenario, including both the Advanced Inductive (hybrid) scenario and the OP2 scenarios at 3.7 MA/2.28 T and 2.7 MA/1.70 T. Section 4 details the results for the OP2 baseline scenario at 4.6 MA/2.28 T. In section 5, the results of the simulations are discussed and compared. Finally, section 6 draws conclusions from the findings.

2. Description of the simulations

The predictions for the ramp-up phase of JT-60SA OP2 hybrid and baseline scenarios, using deuterium as the main ion species, have been performed with the JINTRAC [16] suite of codes. This includes the semi-empirical BgB [22] transport model, which is coupled to the 1.5-D transport solver JETTO [43]. The JETTO code solves the transport equations for the evolution of the plasma current density, main ion density, ion and electron temperatures, and main ion toroidal rotation, averaging these quantities over the magnetic flux surfaces computed by the ESCO equilibrium solver [44]. The impurities are treated interpretatively in all the sections of the paper, except for section 3.4, where the transport of Carbon is evolved by coupling JETTO with the impurity transport code SANCO [56], with the electron density being determined from quasineutrality. The toroidal rotation is always treated predictively, except for the simulation in section 3.1, where it is set interpretatively from the rotation profile used in METIS. However, its effects on transport are not taken into account by the transport model used. The radial coordinate used is the normalized toroidal magnetic flux $\rho_N = \sqrt{\Phi_t/(\pi B_t)}$, which evolves dynamically with the equilibrium magnetic field. Neoclassical transport is computed using NCLASS [58], while the anomalous transport contribution is provided by the BgB transport model.

The BgB model is considered suitable for this study because it has been validated [22, 45, 46] against operational scenarios of JET and JT-60U that are similar to those envisaged for JT-60SA. It tends to slightly overestimate temperatures both in the baseline and hybrid scenarios. Additionally, recent experiments at JET, conducted to support the JT-60SA program, provided an opportunity to further validate the JINTRAC-BgB integrated modelling framework. These experiments involved developing a scenario with non-dimensional plasma parameters (ρ_p^*, β_N, ν^*) similar to those expected for JT-60SA [47]. Preliminary results using JINTRAC-BgB show good agreement between the

experimental and modelled plasma kinetic profiles, as well as the time traces of the main plasma parameters. The average deviation from the experimental temperatures is below 15%, while for the electron density, it remains below 5%.

The choice to use the BgB transport model is motivated not only by its extensive use in JET and JT-60U but also by its low computational burden. This characteristic is crucial given the length of the simulated time interval, which is approximately 20 s. First-principle transport models (e.g. QuaLiKiz [48, 49], TGLF [50]) are also being tested on the JT-60SA similarity experiments at JET [47] for their use in JT-60SA predictions, and the results will be presented in a separate work.

The starting point for the JINTRAC modelling of both the OP2 hybrid and baseline scenarios is a METIS-BgB simulation that covers the ramp-up to the ramp-down phases. Deuterium is used as the main ion species, and carbon is the primary impurity considered. For the baseline scenario, the METIS simulation accounts for the OP2 limitations on NBI and ECRH powers [3]. On the other hand, for the hybrid scenario, the starting point is a METIS simulation [15] of the Advanced Inductive Hybrid scenario (Scenario #4.2 of the JT-60SA Research Plan [1]). As this scenario is planned for the Extended Research Phase, it was necessary to scale it down by reducing the plasma current, magnetic field, heating power, and density to align with the status of the tokamak during OP2.

The simulations begin with a plasma current of approximately 100–500 kA, which increases to the nominal value, initially in a limiter configuration and subsequently in a lower divertor configuration. The METIS simulation provides the waveforms for plasma current (I_p), line-averaged electron density ($< n_e >_{line}$), NBI power (P_{NBI}), and ECRH power (P_{ECRH}), as well as the evolution of the plasma boundary over time. The feasibility of the prescribed plasma shape, including the currents, voltages, and forces on the poloidal field coils, has been assessed through the coupling of METIS with the free-boundary equilibrium code FEEQS [31]. Once the boundary evolution is defined, the fixed-boundary equilibrium solver ESCO [44] computes the equilibrium self-consistently with the evolution of the plasma kinetic profiles.

The initial conditions for the density and temperature profiles are obtained from METIS. The boundary conditions are set at the separatrix, where the electron and ion temperatures are set constant in time and equal to $T_{e,sep} = T_{i,sep} = 100$ eV, while the main ion density $n_{i,sep}$ follows the time evolution provided by METIS. It is important to note that the simulation domain extends from the magnetic axis to the separatrix, and the modelling does not include the scrape-off layer.

A feedback loop, which controls the deuterium gas puff, is used in FRANTIC [51] to sustain the prescribed line averaged electron density. The profiles for NBI and electron cyclotron (EC) heating and current drive are calculated using PENCIL [52] and GRAY [53], respectively. GRAY performs quasi-optical propagation, power absorption, and driven current calculations for a Gaussian beam of EC waves in a general tokamak equilibrium using a beam-tracing approach. This tool reproduces the geometry of the JT-60SA launchers and allows to specify the poloidal and toroidal angles of the steerable mirrors.

The L-H transition is predicted using the Martin scaling [54]. Once the plasma transitions to H-mode, the pedestal is modelled using the empirical continuous edge localised modes (ELMs) model [38]. This approach clamps the normalised pressure gradient α to a critical value α_{crit}, and increases the transport coefficients in the pedestal in order to simulate the effect of ELMs on the pressure gradient. The definition of the normalised pressure gradient used in JETTO differs from the one commonly found in textbooks and is provided below:

$$\alpha_{\mathrm{JETTO}} = \frac{1}{2}\mu_0 r_{\mathrm{omp}}^2 \left| \frac{\mathrm{d}p}{\mathrm{d}\Psi} \frac{1}{B_{\mathrm{omp}}^{\theta}} \right|$$

where Ψ is the poloidal flux, 'omp' stands for 'outboard midplane', and the poloidal component of the magnetic field is computed using the radial and vertical components as:

$$B_{\mathrm{omp}}^{\theta} = \sqrt{B_R\left(r_{\mathrm{omp}}, Z_{\mathrm{mag}}\right)^2 + B_Z\left(r_{\mathrm{omp}}, Z_{\mathrm{mag}}\right)^2}.$$

The width of the pedestal is set, and the pedestal height is taken from METIS, which calculates it according to scaling laws [55].

In this initial phase of the machine, the plasma-facing components are made of carbon, for this reason carbon is assumed to be the dominant impurity. The Z_{eff} profile is assumed to be radially constant. However, the sensitivity of the simulations to impurity transport modelling is evaluated using the impurity transport code SANCO [56]. When using SANCO, a carbon flow rate is set to match the time evolution of Z_{eff}, considering neoclassical transport from NCLASS and anomalous transport from the BgB model. The Z_{eff} value has been verified by COREDIV simulations [57] to ensure compatibility with the boundary condition assumptions and the computed sputtering rates.

When modelling the baseline scenario, the Kadomstev model [59] is used to simulate the sawtooth activity expected for operations with a safety factor profile below one. The sawtooth period is set to 200 ms, which is in the range of what is observed at JET with the C-wall (200–600 ms) [60].

In the hybrid scenario, to prevent numerical issues with the convergence of the equilibrium calculation, the safety factor profile is limited to a maximum value of 3 in the region where $0 < \rho_N < 0.2$. This limitation is necessary due to difficulties encountered by ESCO in computing the equilibrium with hollow current profiles. However, since this affects only a small portion of the plasma, the impact on the predicted profiles is considered negligible.

3. The hybrid scenario

The JT-60SA hybrid scenario envisaged for the Extended Research Phase (ERP), also referred to Advanced inductive in [1], will explore the $q_{95} \sim 4$ (safety factor at the 95% flux surface) regime with reduced plasma current, ranging from 4.6 MA to 3.5 MA [1]. It is anticipated to achieve $\beta_N \sim 3$ (normalized beta) when the auxiliary heating power is between 34 and 37 MW, and a confinement enhancement factor of $H_H \sim$

1.1–1.2. Key characteristics of the hybrid scenario include high β_N values, tailored q (safety factor) profiles, low magnetic shear regions, and $q_{min} > 1$. The JT-60SA hybrid scenario is also known as the Advanced Inductive (Hybrid) scenario or Scenario #4.2 in the JT-60SA Research Plan [1].

The hybrid scenario planned for Operation Phase 2 (OP2) of JT-60SA will approach the target operational parameters in a staged manner, starting with lower plasma current, magnetic field, and heating power.

In this study, the OP2 hybrid scenario is modelled by progressively scaling down the plasma current, magnetic field, heating power, and density from the Advanced Inductive (hybrid) scenario, which has been extensively studied in [23, 32, 41]. Concurrently, an optimization process is applied to available engineering parameters—such as the ramp rates of plasma current and electron density, and the timing of NBI—to achieve a q profile above one throughout the entire plasma radius, while maintaining a low magnetic shear region.

For the Advanced Inductive (Hybrid) scenario, the available NBI and ECRH power will be $P_{NBI} = 30$ MW and $P_{ECRH} = 7$ MW. In contrast, during Operation Phase 2 (OP2), the maximum available NBI and ECRH power will be $P_{NBI} =$ 23.5 MW (in Deuterium) and $P_{ECRH} = 3$ MW for 5 s (with 1.5 MW available for 100 s). The duration of OP2 pulses will be strongly influenced by the need to preserve the integrity of the divertor, which is inertially cooled during this initial phase. Similarly, the operational duration of ECRH power will depend on the cooling capacity of the transmission line components. The reduced heating and current drive power during OP2 will influence the shaping of the q profile, particularly at lower plasma current and density.

3.1. ERP Advanced inductive (hybrid) scenario

The Advanced Inductive (hybrid) scenario envisaged for the Extended Research Phase (ERP), referred to as Scenario #4.2 in [1], is an H-mode characterized by $I_p = 3.5$ MA, $B_t = 2.28$ T, $q_{95} \sim 4.4$, $\beta_N \sim 3$, $H_H \sim 1.2$, and a Greenwald fraction of $n_e/n_{GW} = 0.8$. The NBI power of $P_{NBI} = 30$ MW is allocated as follows: 10 MW from negative-ion-based NBI (N-NBI) with a beam energy of 500 keV (5 MW unit^{-1}) and 20 MW from positive-ion-based NBI (P-NBI) with a beam energy of 85 keV (2 MW unit^{-1}). The P-NBI consists of 12 units—8 with perpendicular injection and 4 with tangential injection (2 co-current and 2 counter-current)—providing heating primarily to ions, torque control, and contributing to current drive. The N-NBI comprises 2 units that mainly provide heating to electrons and drive a high off-axis current. The ECRH power is $P_{ECRH} = 7$ MW at 138 GHz in X-mode to achieve absorption at the $n = 2$ harmonic. In JINTRAC, the critical pressure gradient α_{crit} used to match the pedestal of METIS is set to 1.8 (note that the JETTO definition for the α_{crit} differs from the usual one, as reported in section 2). The Z_{eff} value of 2.1 is consistent with the boundary conditions and sputtering rates computed by COREDIV simulations [57]. As detailed in section 2, the evolution of I_p is imposed in JINTRAC, while a feedback loop on the Deuterium gas puff ensures the prescribed evolution of $< n_e >_{line}$ from METIS.

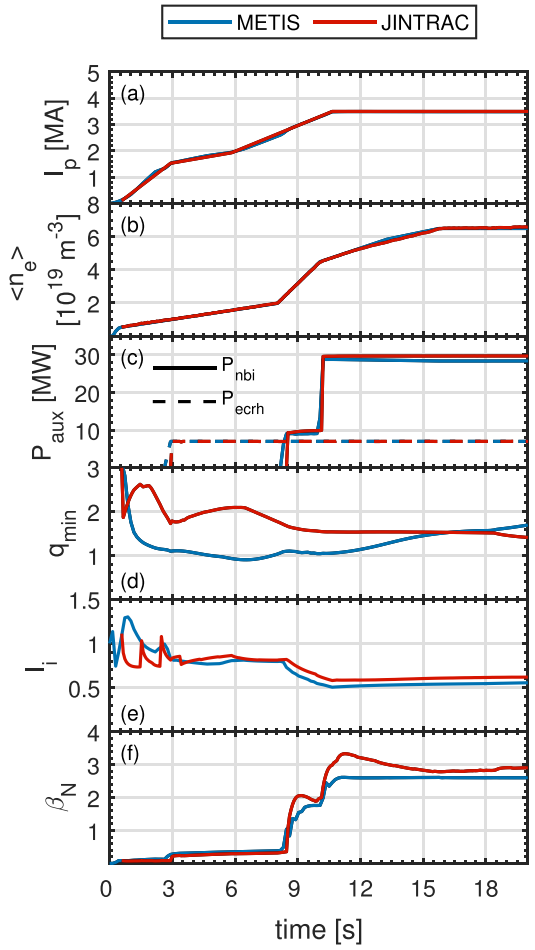

Figure 2. Time evolution of the plasma current (I_p), line averaged electron density ($< n_e >_{line}$), NBI end ECRH powers (P_{nbi}, P_{ecrh}), minimum value of the safety factor (q_{min}), internal inductance (l_i) and normalised beta (β_N) computed by the 0.5-D code METIS (blue) and the 1.5-D code JINTRAC (red) for the Advanced inductive (hybrid) scenario (Scenario #4.2).

Using the BgB transport model, the current density (J_z), the main ion density (n_D), and the electron and ion temperatures (T_e and T_i) are predicted, while the rotation is kept interpretative and set equal to that from METIS. For the size and configuration of the plasma refer to [1, p 16].

The waveforms of the plasma current (I_p), line-averaged electron density ($< n_e >_{line}$), NBI and ECRH powers (P_{NBI}, P_{ECRH}), minimum value of the safety factor (q_{min}), internal inductance (l_i), and normalized beta (β_N) are shown in figure 2.

The plasma kinetic profiles (n_e, T_e, T_i) at three different times during the simulation interval are shown in figure 3 for both METIS and JINTRAC. The profiles are displayed at:

- 1.5 s, when the simulations had sufficient time ($t > 3\tau_E$) to relax from their initial conditions;
- 8 s, after the ECRH injection and before the switch-on of the NBI;
- 20 s, approximately 5 s into the flat-top phase, which corresponds to the end of the simulated time interval.

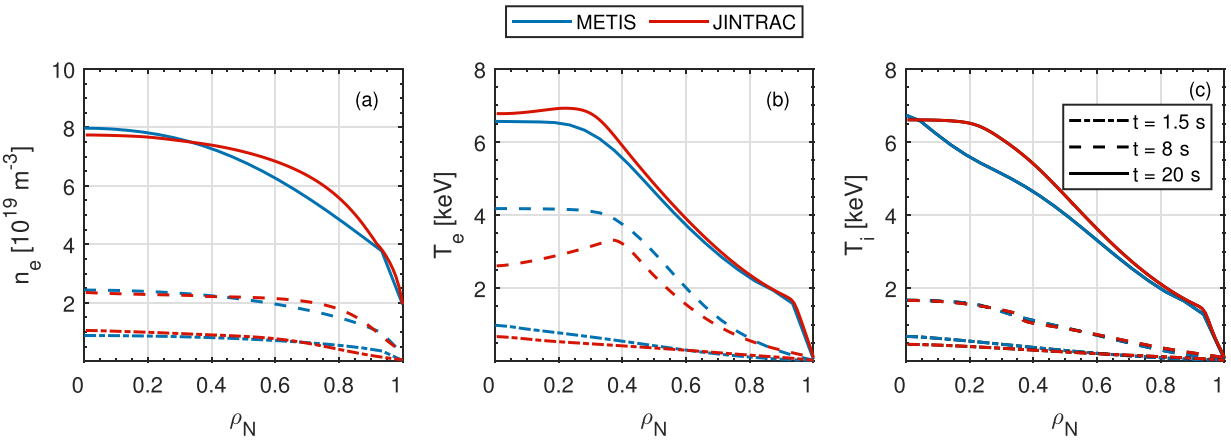

Figure 3. Profiles of the electron density (n_e), electron temperature (T_e) and ion temperature (T_i) computed by JINTRAC (red) and METIS (blue) for the Advanced inductive (hybrid) scenario (Scenario #4.2). The quantities are shown at three different time of the simulation: at the beginning of the ramp-up phase (1.5 s), when the initial conditions had enough time to relax; after the ECRH injection and before the switching-on of the NBI (8 s); at the end of the simulation and ∼5 s into the flat-top phase (20 s).

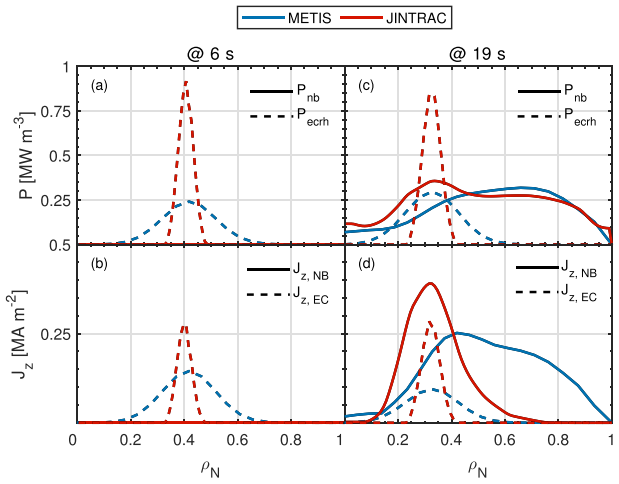

Figure 4. Heating (top) and current drive (bottom) deposition profiles computed by JINTRAC (red) and METIS (blue) for the Advanced inductive (hybrid) scenario (Scenario #4.2). The profiles are shown both during the ramp-up phase (left) and during the flat-top phase (right).

Overall, there is good agreement between the two codes. The main differences observed can be attributed to variations in the heating deposition profiles, which predominantly affect $T_{e,i}$, and in the current deposition profiles, which influence the q profile and, consequently, the transport. JINTRAC simulations where the METIS density is imposed indicate that its effect on the temperature profiles is minimal. In contrast, when imposing the same heating deposition profiles, the most substantial impact on T_e and T_i arises from the NBI profile, while the ECRH is slightly influencing the core T_e profile.

In figure 4, a comparison is shown between the deposition profiles of the NBI and ECRH at two different times: during the ramp-up (6 s) and the flat-top phase (19 s). The steering angles of the EC launchers in the GRAY code are adjusted to match both the centre of the deposition profile (by modifying the poloidal angle α) and the EC current-driven fraction $f_{ECCD} = I_{ECCD}/I_p$ (by modifying the toroidal angle β) of METIS, which prescribes a Gaussian-like profile. The optimal centre of the profile is located around $\rho_N \sim 0.33$, balancing a high central T_e and a q profile above unity, as reported in [32].

Since METIS shifts the EC centre from $\rho_N = 0.40$ to $\rho_N = 0.33$ during the ramp-up phase, a corresponding shift in the poloidal injection angle from $\alpha = 12°$ to $\alpha = 18°$ is applied in GRAY to account for this change, while keeping the toroidal injection angle constant at $\beta = 12°$. The heating and current profiles computed by GRAY are narrower and have a higher peak compared to the Gaussian-like profiles imposed by METIS, which explains the differences in T_e seen in box (b) of figure 3.

Another significant difference between the two codes lies in the NBI current-driven profile $J_{z,NB}$ (box (d) of figure 4), computed by a simple model in METIS and by the PENCIL code in JINTRAC. The position of the peak of the NBI deposition in JINTRAC is close to the ECRH one, whereas a broader profile is found in METIS. The overlap of the peaks of the ECRH and NBI in JINTRAC leads to a hollow total current density profile at the end of the flat-top phase, as shown in figure 5, which, in turn, results in a q profile with a negative shear region.

Moreover, due to the flat pressure profile computed by JINTRAC-BgB between $0 < \rho_N < 0.2$, the bootstrap current contribution in that region is found to be close to zero (see figure 5), which differs from the results obtained with METIS.

A summary of the main plasma parameters computed by METIS and JINTRAC, averaged during the flat-top phase, is presented in table 1. These values are compared with the reference parameters computed by ACCOME and reported in the Research Plan [1, p 16].

The parameters computed by JINTRAC and METIS are generally in close agreement and align well with the reference parameters calculated by ACCOME. The largest discrepancy between the two codes is found in the higher non-inductive current fraction predicted by METIS, with a $\Delta = f_{ni,METIS} -$

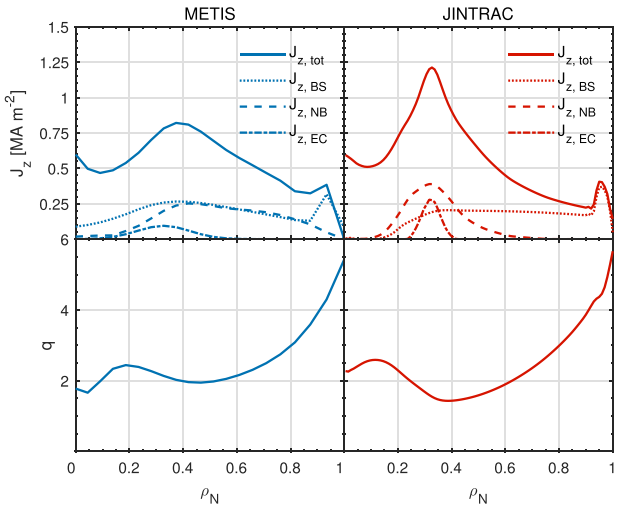

Figure 5. Composition of the current density (J_z) profile (top) and safety factor profile (bottom) for the Advanced inductive (hybrid) scenario (Scenario #4.2) during the flat-top phase computed by METIS (left) and JINTRAC (right). The total current density ($J_{z,\mathrm{tot}}$), the bootstrap current density ($J_{z,\mathrm{BS}}$), the NBI current density ($J_{z,\mathrm{NB}}$) and the EC current density ($J_{z,\mathrm{EC}}$) are shown.

Table 1. Comparison between the plasma parameters computed by the 1.5-D code JINTRAC, the 0.5-D code METIS and the reference values computed by the 2D free-boundary equilibrium code ACCOME (table 1-3 of [1]) for the Advanced inductive (hybrid) scenario (Scenario #4.2).

	Advanced inductive hybrid scenario (Scenario #4.2)		
Main ion	JINTRAC D	METIS D	Reference D
B_t (T)	2.28	2.28	2.28
I_p (MA)	3.50	3.50	3.50
f_bs (%)	41.46	39.90	40.00
f_ni (%)	58.73	73.53	58.00
f_gw (%)	76.91	76.21	80.00
q_{95}	4.37	4.63	4.40
P_nbi (MW)	29.72	28.39	30
P_ecrh (MW)	7.00	7.00	7.00
P_rad (MW)	2.11	2.70	—
$n_{\mathrm{e},0}$ (10^{19} m^{-3})	7.70	7.97	8.40
$< n_{\mathrm{e},0} >$ (10^{19} m^{-3})	6.57	6.49	6.90
$T_{\mathrm{e},0}$ (keV)	6.80	6.51	7.50
$< T_\mathrm{e} >$ (keV)	3.71	3.51	3.70
$T_{\mathrm{i},0}$ (keV)	6.61	6.69	7.50
$< T_\mathrm{i} >$ (keV)	3.39	3.03	3.70
W_th (MJ)	12.98	11.55	13.40
$\beta_\mathrm{N}, \beta_\mathrm{p}$	2.90, 1.43	2.61, 1.05	3.00, 1.15
τ_E (S)	0.37	0.34	0.36
H_{98}	1.22	1.20	1.20
Z_eff	2.10	2.10	—
neutrons (10^{16} s^{-1})	5.26	4.30	—

$f_{\mathrm{ni,JINTRAC}} = 15\%$. This difference arises solely from the lower beam-driven current calculated by JINTRAC, as the bootstrap current fraction and EC-driven current fraction are nearly identical between the two codes. Notably, the computed $H_{98} \sim 1.2$ value by JINTRAC is in agreement with the assumed values in both METIS and ACCOME. Additionally, the average temperatures ($\langle T_\mathrm{e} \rangle, \langle T_\mathrm{i} \rangle$) prediction show a small difference of only 5% for $\langle T_\mathrm{e} \rangle$ and 10% for $\langle T_\mathrm{i} \rangle$. Comparing these results with the flat-top phase modelling presented in [23], there is a consistent agreement across the various modelling codes used to predict the JT-60SA hybrid scenario. This agreement provides confidence in the extrapolation of this scenario to lower current and field values in preparation for OP2.

3.2. OP2 hybrid scenario at 3.7 MA/2.28 T

The first version of the JT-60SA hybrid scenario foreseen for Operation Phase 2 (OP2) is obtained by scaling down the auxiliary heating power of the Advanced inductive (hybrid) scenario, shown in section 3.1, from 37 MW to 19 MW. The plasma current is slightly changed from 3.5 MA to 3.7 MA, while the magnetic field is kept constant at 2.28 T. Since the Greenwald density fraction n_e/n_{GW} is also kept constant at 0.8, the line-averaged electron density $< n_e >_{line}$ is slightly increased from 6.6×10^{19} to 7.0×10^{19} m^{-3} to account for the increase in I_p.

The total NBI heating power of $P_{NBI} = 16$ MW is divided into 10 MW of N-NBI and 6 MW of P-NBI, while the total ECRH power is $P_{ECRH} = 3$ MW at 138 GHz in X-mode. In this initial phase, four gyrotrons with an output power of 1 MW each will be available: two gyrotrons with a pulse duration of 100 s (at 82/110/138 GHz with steerable launchers) and the other two with a pulse duration of 5 s (one at 82/110/138 GHz and the other at 110 GHz). Taking into account the transmission loss of about 25%, an injection power of $P_{ECRH} = 3$ MW will be possible at 110 GHz and 2.25 MW at 138 GHz. However, in the modelling of the hybrid scenario at 3.7 MA presented in this paper, it is assumed that all four gyrotrons can operate at 138 GHz.

The maximum ECRH power of 3 MW for 5 s is used in the initial part of the ramp-up phase (from ∼3 to 8 s) to slow down the current diffusion, and it is then scaled down to 1.5 MW for the remaining part of the simulation.

In figure 6, the comparison between the JINTRAC-BgB Advanced inductive (hybrid) scenario and its scaled-down version in view of OP2 (not yet optimized) is shown. By looking at the time traces of the simulation, it is clear the importance of having a high ECRH power in the initial phase of the ramp-up to maintain the q profile above one, before the NBI injection and the transition to H-mode. In fact, with a reduced ECRH power of 3 MW and a reduced current drive capability of the 2 gyrotrons without steerable launchers, the q_{min} starts decreasing from 3 s and goes below one at ∼7.96 s.

A staged optimization of the ramp-up phase is carried out to yield a safety factor profile above one at the L-H transition and to maintain it until the end of the simulated time interval. This is done by acting first on the plasma current ramp, then on the NBI switching-on time, and lastly on the electron density ramp, which are characteristics of the scenario that can be somewhat controlled when operating a tokamak. The modifications applied at each stage of the optimization process are then maintained for the following steps.

In figure 7, the effect on the l_i and q_{min} of a slower and faster I_p ramp in the initial phase of the scenario (from 0.5 to 6 s) is shown. The waveforms of the heating power and density are kept fixed and equal to the reference case. It seems that a slower current ramp in the initial phase (from 0.5 to 6 s), followed by a faster ramp in the second phase (from 6 to 10 s), is beneficial in keeping the q profile above one until the NBI is switched on. However, a limit exists in pushing towards an even slower I_p ramp in the initial phase, since it would force a fast I_p ramp (greater than 0.5 MA s^{-1}) in the second phase, which might trigger deleterious MHD activity.

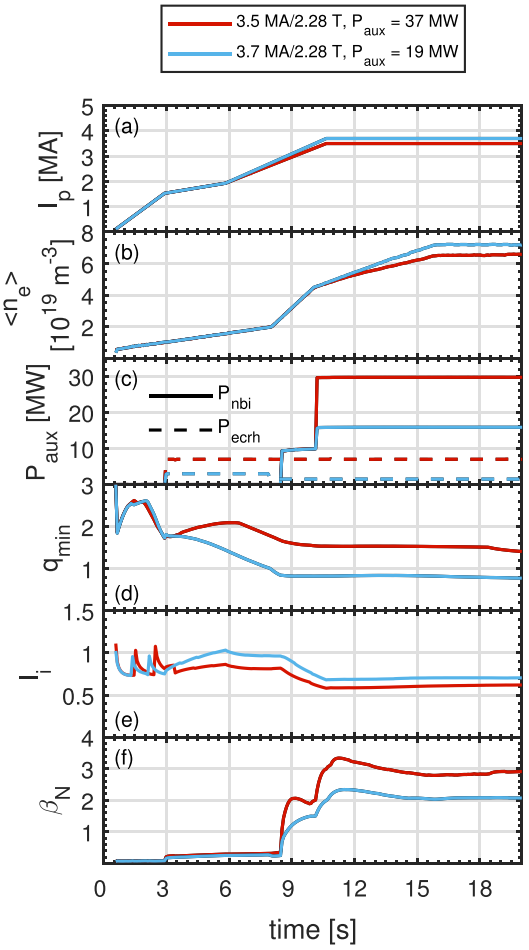

Figure 6. Time evolution of the plasma current (I_p), line averaged electron density ($< n_e >_{line}$), NBI end ECRH powers (P_{nbi}, P_{ecrh}), minimum value of the safety factor (q_{min}), internal inductance (l_i) and normalised beta (β_N) computed by JINTRAC for the Advanced inductive (hybrid) scenario at 37 MW (red) and the 3.7 MA OP2 hybrid scenario at 19 MW (light blue). The OP2 hybrid scenario shown here has not been optimized yet.

Despite the improvement in q_{min} at the L-H transition when using the optimized I_p ramp, the value goes below one at ∼18 s, and further optimization is needed.

After having explored the effect of a modified I_p ramp, the effect of the NBI timing on the q_{min} is assessed in figure 8. The reference METIS time of NBI injection, $t_0 = 8.46$ s, is anticipated by 300 and 600 ms. An earlier NBI timing, which leads to an earlier L-H transition, allows freezing the q profile at a higher value and maintaining it for longer. However, when anticipating the NBI by 600 ms (green line in figure 8), the density at the NBI switch-on is lower, leading to high NBI shine-through losses ($P_{ST} \sim 1.3$ MW).

In order to decrease the shine-through losses, the value of $< n_e >_{line}$ at the time of NBI injection is increased by 15%, 30% and 50% with respect to the reference METIS value of 2×10^{19} m^{-3}, and the results are shown in figure 9. It is found that a 30% higher value of $< n_e >_{line}$ at 8 s, leading to a density ramp of 2.7×10^{18} m^{-3}s^{-1} (blue line in figure 9), is a good compromise between a $q_{min} > 1$ for the whole simulated time

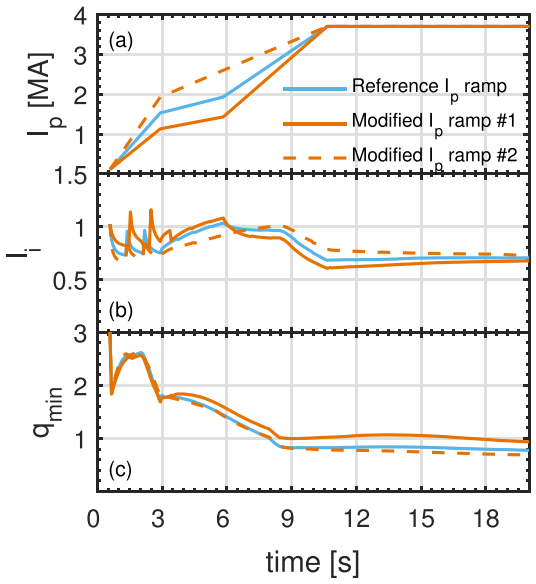

Figure 7. Effect of a faster and slower plasma current ramp on the l_i and q_{min}. The modified I_p ramp #1 (solid orange line) is chosen for its beneficial effect on the q_{min}.

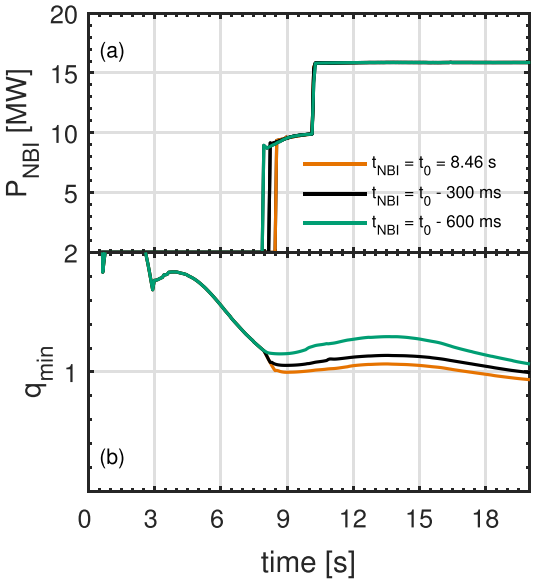

Figure 8. Effect of the timing of the NBI injection on the q_{min}, where the reference value of 8.46 s is anticipated by 300 and 600 ms. The earlier NBI injection (green line) allows an earlier L-H transition and the freezing of the q profile at a value greater than one, which is maintained until the end of the simulated time interval. A drawback of this are the higher shine-through losses at lower density.

interval and shine-through losses $P_{ST} < 0.65$ MW. A higher $< n_e >_{line}$ value would lead to a lower T_e in the initial phase of the ramp-up and a faster current diffusion.

The time traces of the optimized OP2 hybrid scenario at 3.7 MA/2.28 T, $P_{aux} = 19$ MW and 0.8 of Greenwald fraction (using the line averaged electron density) are shown in figure 10, together with the $n_e/n_{GW} = 0.6$ and 0.4 versions of the scenario. The values of the density at the top of the pedestal

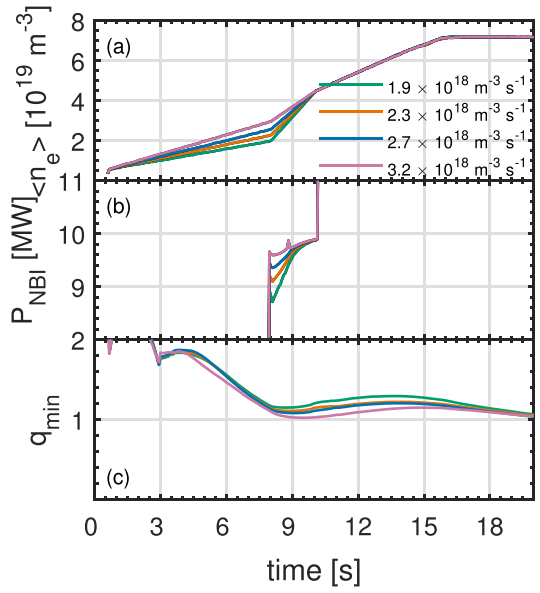

Figure 9. Effect of different density ramps on the NBI shine-through losses and on the q_{min}. The $< n_e >_{line}$ value at the NBI injection is increased by 15, 30 and 50 % with respect to the reference value used in METIS. An optimum is found with a density ramp of 2.7×10^{18} m^{-3}s^{-1} (blue).

for $f_{GW} = 0.6$ and 0.4 are obtained by scaling the line averaged electron density while keeping the same α_{crit} value in the ETB used at $f_{GW} = 0.8$. The plasma kinetic profiles (n_e, T_e, T_i) at three different times are shown in figure 11, while the flat-top profiles of the heating power, current drive, and safety factor are shown in figure 12.

It is important to highlight that when $n_e/n_{GW} = 40\%$, the scenario appears to be over-powered and over-driven. In other words, the desired hybrid-like q profile is achieved more easily at a reduced N-NBI power. This occurs because the highly energetic N-NBI beams, at lower density, drive a strong off-axis current, which leads to a reversal in the q profile, as shown by the black line in box (c) of figure 12.

A possible solution to this issue is investigated by trying different combinations of Negative-ion-based and Positive-ion-based NBI. The cases tested include: (i) $P_{N-NBI} = 0$ MW and $P_{P-NBI} = 13.5$ MW, which represents the maximum P-NBI power available for OP2; (ii) $P_{N-NBI} = 5$ MW from the upper injector (U) and $P_{P-NBI} = 11$ MW; (iii) $P_{N-NBI} = 5$ MW from the lower injector (L) and $P_{P-NBI} = 11$ MW. The resulting $J_{z,NB}$ and q profiles are shown in figure 13, compared to the reference case (solid black line) with $P_{N-NBI} = 10$ MW and $P_{P-NBI} = 6$ MW. A monotonically increasing q profile above unity is achievable for the $n_e/n_{GW} = 0.4$ case with 0 MW of N-NBI. However, if 5 MW of N-NBI are used, the different geometries of the upper and lower N-NBI lead to varying degrees of broadening in the q profile, with some regions exhibiting negative shear. When the upper N-NBI injector is used, the negative shear region is less broad compared to the lower N-NBI injector case, making it a better candidate for this scenario.

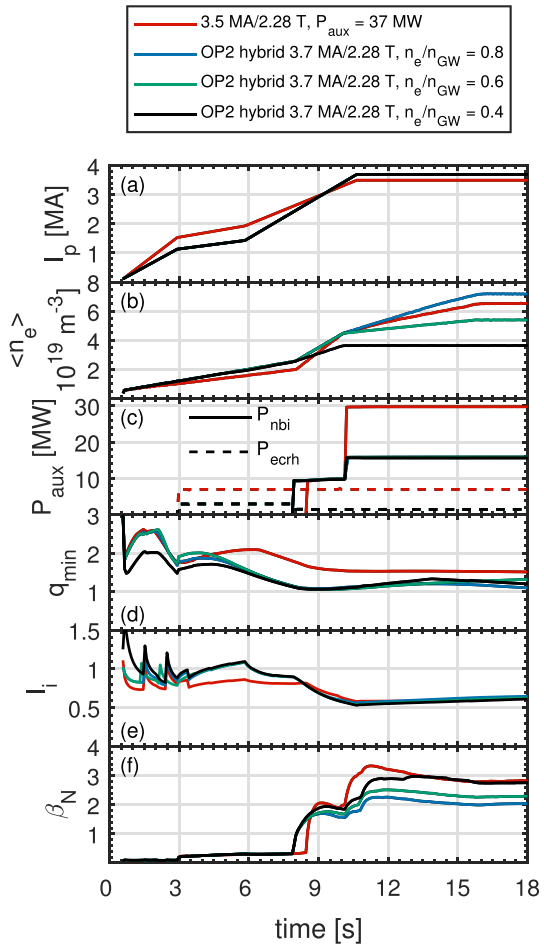

Figure 10. Time evolution of the plasma current (I_p), line averaged electron density ($< n_e >_{line}$), NBI end ECRH powers (P_{nbi}, P_{ecrh}), minimum value of the safety factor (q_{min}), internal inductance (l_i) and normalised beta (β_N) computed by JINTRAC for the optimized 3.7 MA/2.28 T OP2 hybrid scenario at three Greenwald density fractions: 0.8 (blue), 0.6 (green), 0.4 (black). These are compared with the Advanced inductive (hybrid) scenario (Scenario #4.2) at 37 MW (red).

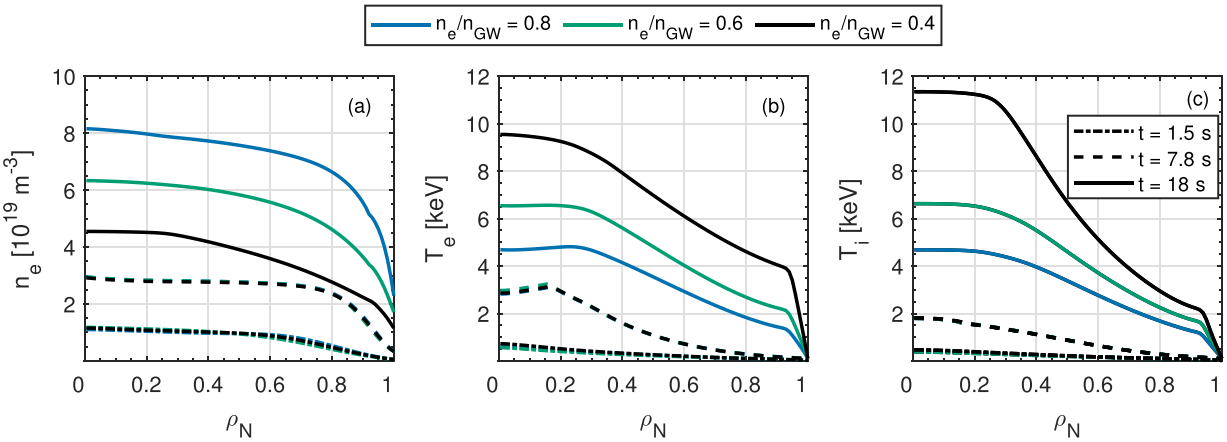

Figure 11. Profiles of the electron density (n_e), electron temperature (T_e) and ion temperature (T_i) computed by JINTRAC-BgB for the optimized OP2 hybrid scenario at 3.7 MA/2.28 T. The quantities are shown at three different time of the simulation: at the beginning of the ramp-up phase (1.5 s), when the initial conditions had enough time to relax; after the ECRH injection and before the switching-on of the NBI (7.8 s); in the flat-top phase (18 s). Three values of the Greenwald density fraction are compared: 0.8 (blue), 0.6 (green), 0.4 (black).

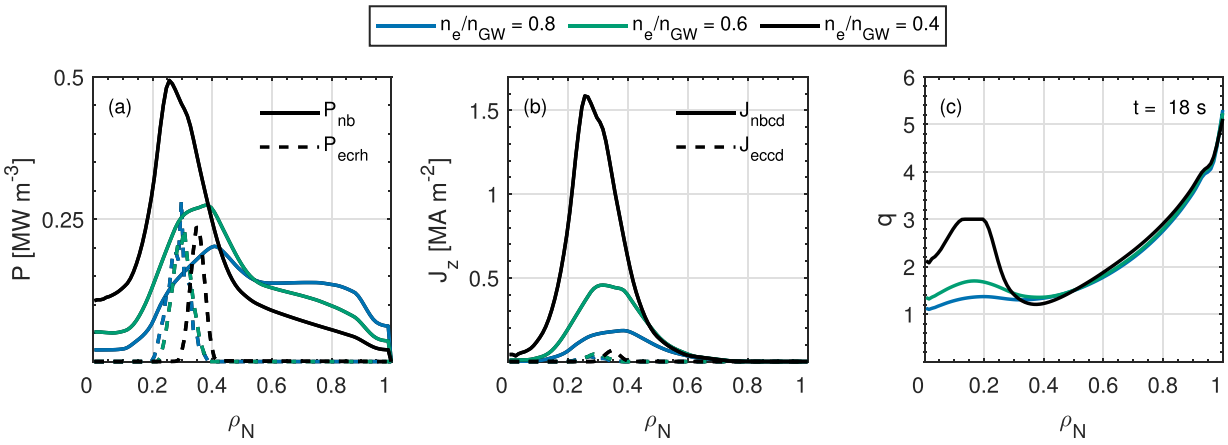

Figure 12. Profiles of the NBI and ECRH powers (*a*), NBI and EC current densities (*b*) and safety factor (*c*) computed by JINTRAC-BgB for the optimized OP2 hybrid scenario at 3.7 MA/2.28 T. Three values of the Greenwald density fraction are compared: 0.8 (blue), 0.6 (green), 0.4 (black).

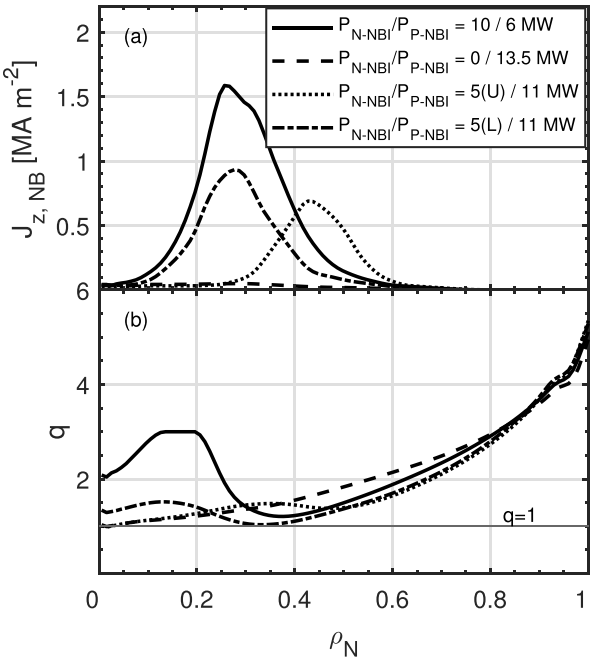

Figure 13. Profiles of the NBI driven current $J_{z,\mathrm{NB}}$ (*a*) and safety factor q (*b*) in the flat-top phase for the optimized 3.7 MA/2.28 T OP2 hybrid scenario at $n_\mathrm{e}/n_\mathrm{GW} = 0.4$. Various combinations of the NBI units are investigated to yield a q profile above one with a low magnetic shear region.

3.3. OP2 hybrid scenario at 2.7 MA/1.7 T

The second version of the hybrid scenario planned for Operation Phase 2 (OP2) is a 2.7 MA/1.70 T H-mode, with a safety factor of $q_{95} \sim 4.3$ and an auxiliary heating power of $P_\mathrm{aux} = 19$ MW. The starting point for modelling this scenario is the optimized 3.7 MA/2.28 T hybrid scenario described in section 3.2. This reference scenario is scaled down to a lower plasma current and magnetic field while maintaining constant auxiliary heating power for three different Greenwald fraction values ($n_\mathrm{e}/n_\mathrm{GW} = 0.8, 0.6, 0.4$).

One of the key advantages of this scenario for OP2 is that it enables easier exploration of the high β_N regime with the same heating power (19 MW), at a reduced magnetic field (1.7 T). Additionally, the gyrotron frequency is adjusted from 138 GHz to 110 GHz to ensure absorption at the second harmonic ($n = 2$) for the 1.70 T magnetic field.

Figures 14 and 15 show the time traces and plasma kinetic profiles ($n_\mathrm{e}, T_\mathrm{e}, T_\mathrm{i}$) for the OP2 hybrid scenario at 2.7 MA/1.7 T, computed for three values of the $n_\mathrm{e}/n_\mathrm{GW}$ ratio (0.8, 0.6, and 0.4) using JINTRAC-BgB. In these simulations, the optimized current ramp, density ramp, and NBI timing obtained at higher current, as described in section 3.2, are preserved. This ensures that q_min remains above one at all densities. As expected, the β_N is higher than the one computed for the 3.7 MA scenario, reaching values as high as 3 in the lower density case.

However, when the Greenwald fraction drops to 60% and 40%, the strong current driven by the 10 MW of N-NBI may become too large to sustain the hybrid scenario, leading to a highly reversed q profile, as seen in box (*c*) of figure 16, particularly in the lower density case. As was done for the 3.7 MA scenario, various combinations of the Negative and Positive-ion-based NBI were tested to produce a q profile that remains above one and has a low magnetic shear region. The results for $n_\mathrm{e}/n_\mathrm{GW} = 0.4$ are presented in figure 17. When the N-NBI is completely switched off, the q profile increases monotonically but with $q_\mathrm{min} < 1$. The optimum configuration appears to be when only the upper N-NBI launcher (5 MW) is used, driving a current centred around $\rho_\mathrm{N} \sim 0.5$, which helps broaden the q profile and keep it above unity.

A scan of the steering angles of the EC launchers was also conducted to evaluate the sensitivity of the q profile to the EC current density profile. The poloidal angle (α) and toroidal angle (β) of the steerable mirrors were varied one at a time while keeping the other fixed, as shown in figures 18 and 19. The poloidal angle α primarily affects the centre of the deposition profile, whereas the toroidal angle β has a greater influence on the EC-driven current, which can reach up to 50.7 kA for $\alpha = \beta = 20°$. However, the overall effect on the q profile

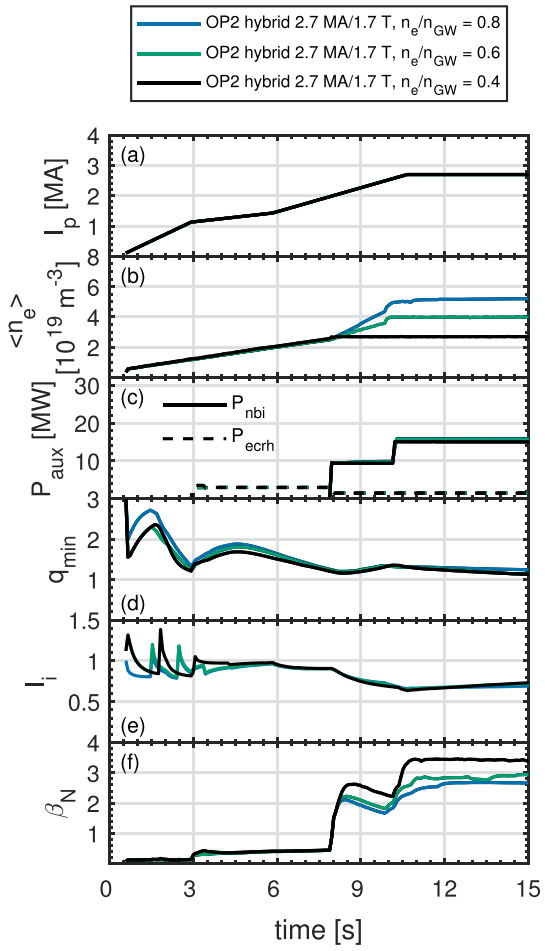

Figure 14. Time evolution of the plasma current (I_p), line averaged electron density ($< n_\mathrm{e} >_\mathrm{line}$), NBI end ECRH powers ($P_\mathrm{nbi}, P_\mathrm{ecrh}$), minimum value of the safety factor (q_min), internal inductance (l_i) and normalised beta (β_N) computed by JINTRAC for the 2.7 MA/1.70 T OP2 hybrid scenario at three Greenwald density fractions: 0.8 (blue), 0.6 (green), 0.4 (black).

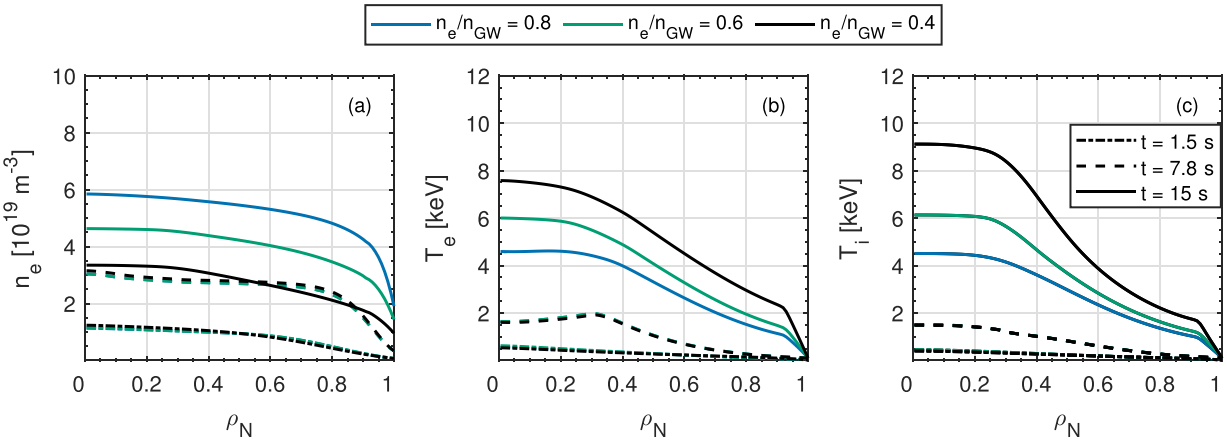

Figure 15. Profiles of the electron density (n_e), electron temperature (T_e) and ion temperature (T_i) computed by JINTRAC-BgB for the OP2 hybrid scenario at 2.7 MA/1.70 T. The quantities are shown at three different time of the simulation: at the beginning of the ramp-up phase (1.5 s), when the initial conditions had enough time to relax; after the ECRH injection and before the switching-on of the NBI (7.8 s); in the flat-top phase (15 s). Three values of the Greenwald density fraction are compared: 0.8 (blue), 0.6 (green), 0.4 (black).

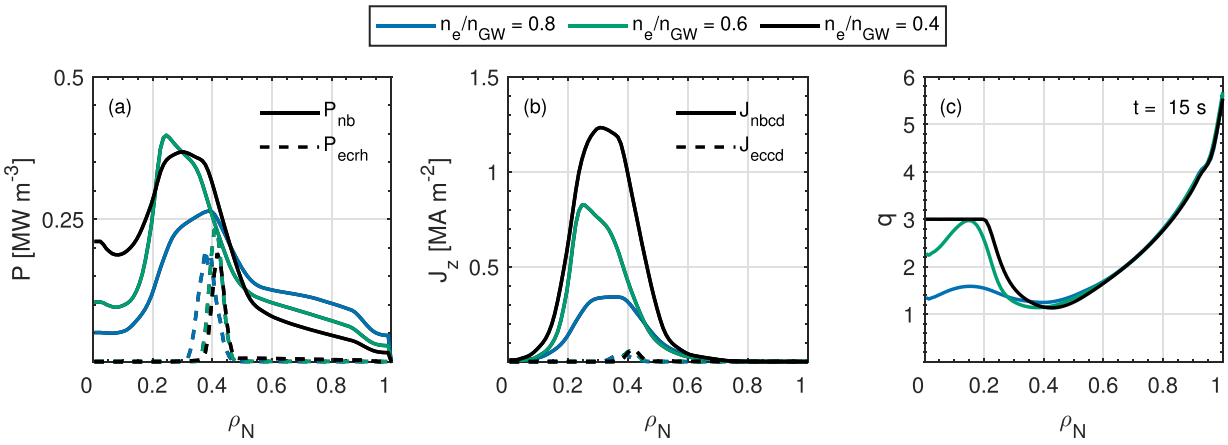

Figure 16. Profiles of the NBI and ECRH powers (*a*), NBI and EC current densities (*b*) and safety factor (*c*) computed by JINTRAC-BgB for the OP2 hybrid scenario at 2.7 MA/1.70 T. Three values of the Greenwald density fraction are compared: 0.8 (blue), 0.6 (green), 0.4 (black).

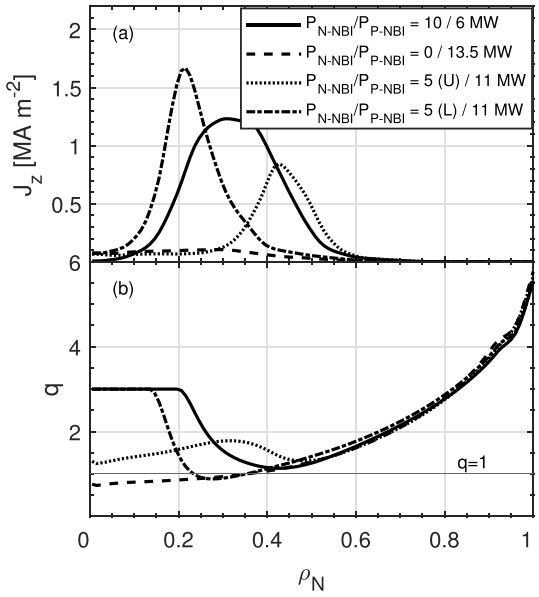

Figure 17. Profiles of the NBI driven current $J_{z,\mathrm{NB}}$ (*a*) and safety factor q (*b*) in the flat-top phase for the 2.7 MA/1.70 T OP2 hybrid scenario at $n_\mathrm{e}/n_\mathrm{GW} = 0.4$. Various combinations of the NBI units are investigated to yield a q profile above one with a low magnetic shear region.

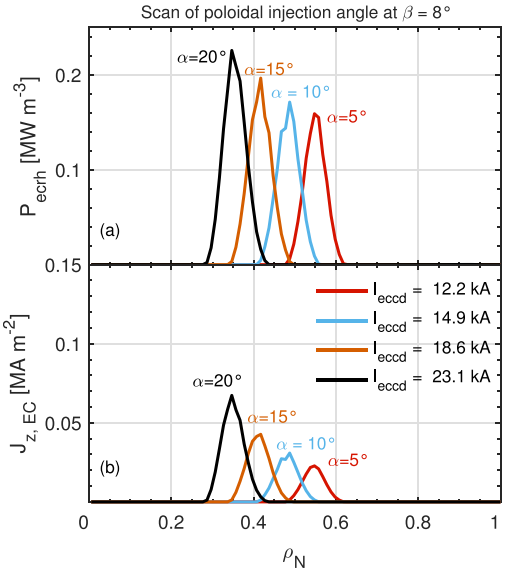

Figure 18. Scan of the poloidal injection angle (α) of the EC beam at constant toroidal angle ($\beta = 8°$) and effect on the heating (*a*) and current (*b*) deposition profiles. The poloidal angle is mostly affecting the position of the centre of the deposition profile.

remains around $\sim$10%, given the relatively low EC-driven current and the lower P_ECRH compared to the N-NBI power.

3.4. Sensitivity to the transport of impurities

The transport of carbon is predicted using the impurity transport code SANCO [56] to evaluate its impact on the predicted q profile. Previous work conducted at JET on neon seeded plasmas [62] has demonstrated that the impurity transport predicted by SANCO not only aligns with experimental data in terms of Z_eff, P_rad, and impurity composition, but can also be relied upon for predicting light impurity density profiles [63].

In this initial phase, JT-60SA will be equipped with an inertially cooled carbon divertor and a carbon wall, for this reason carbon is assumed to be the dominant impurity. In previous simulations, impurities were treated interpretatively, with fixed and radially constant profiles for Z_eff and P_rad. However, when using SANCO, the transport of carbon is computed, incorporating both neoclassical contributions from NCLASS and anomalous contributions from BgB.

A carbon source is prescribed with a rate that ranges from 1.4 to 0.2×10^{19} s^{-1} to match the Z_eff envisaged in the METIS simulation. This rate is adjusted based on the plasma density ramp and the desired Z_eff value.

Figure 20 shows a comparison between simulations with interpretative and predicted impurities for the OP2 hybrid scenario at 2.7 MA/1.70 T ($n_\mathrm{e}/n_\mathrm{GW} = 0.4$). The Z_eff profile computed by SANCO is found to be higher at the edge and lower in the core compared to the radially constant $Z_\mathrm{eff} = 2.1$

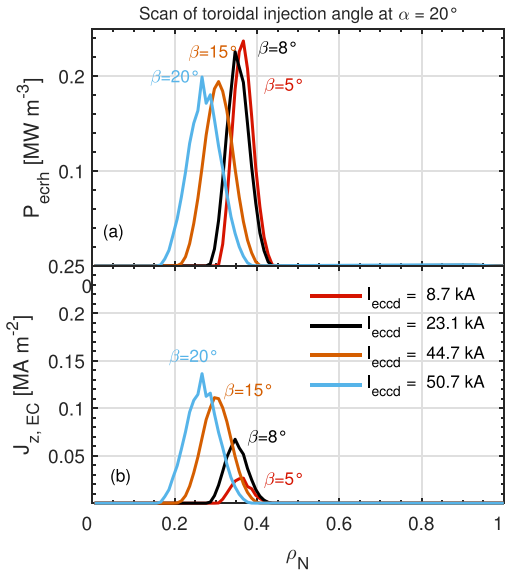

Figure 19. Scan of the toroidal injection angle (β) of the EC beam at constant poloidal angle ($\alpha = 20°$) and effect on the heating (a) and current (b) deposition profiles. The toroidal angle is mostly affecting the intensity of the EC driven current.

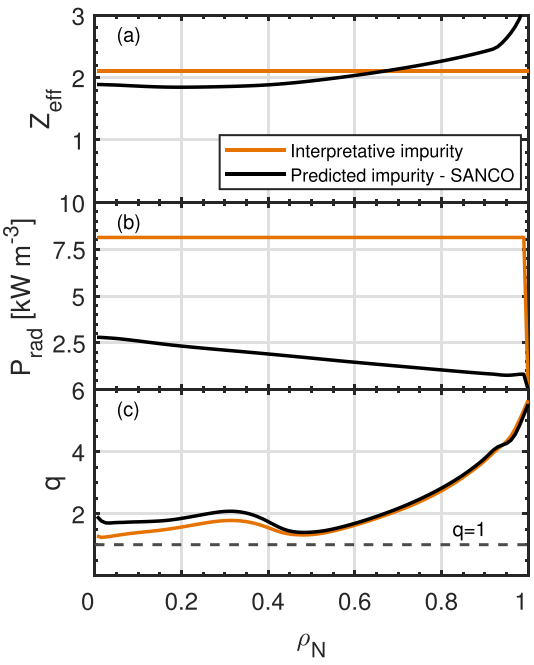

Figure 20. Comparison of interpretative and predictive impurity behaviour for the OP2 hybrid scenario at 2.7 MA/1.70 T ($f_{GW} = 0.4$) using the SANCO code. (a) Effective charge Z_{eff} profile, (b) radiated power density (P_{rad}) profile, and (c) safety factor (q) profile as a function of normalized radius.

profile. This results in lower plasma resistivity and slower current diffusion in the core, leading to a slightly higher q profile in the JINTRAC-SANCO-BgB simulation. Additionally, the radiation profile is almost four times lower than the reference value, which increases T_e in the core and further contributes to the reduction in current diffusion.

Although the q profile undergoes modification, the change is only approximately 20%, and the differences in the main plasma parameters between the two cases are even smaller, ranging from 5% to 10%. Similarly, when modelling the transport of C in the OP2 hybrid scenario at 3.7 MA/2.28 T ($n_e/n_{GW} = 0.4$), the impact on the q profile in the core is about 10% while the q_{min} value is 35% higher. This indicates that the optimization process described in section 3.2, aimed at achieving a $q_{min} > 1$, remains valid and can be considered conservative.

4. The baseline scenario

The JT-60SA baseline scenario for Operation Phase 2 (OP2) is a 4.6 MA/2.28 T H-mode, with $q_{95} \sim 3$ and an auxiliary heating power of $P_{aux} = 17.5$ MW. As JT-60SA is the largest superconducting tokamak capable of achieving ITER-like shapes, demonstrating the ITER baseline H-mode scenario on JT-60SA is crucial before the start of ITER operations. The high confinement at high current will provide a 'workhorse' scenario for operations at low collisionality. Additionally, different versions of this scenario, at both high and low densities, will be used by the JT-60SA Experiment Team to address specific ITER needs, such as high-density termination, P_{LH} threshold studies, and runaway electron investigations [1, p 52].

The NBI power of 16 MW is divided into 10 MW of Negative-ion-based NBI and 6 MW of Positive-ion-based NBI, similar to the OP2 hybrid scenario. Additionally, the ECRH power is 1.5 MW at 138 GHz in X-mode, using steerable launchers. An $\alpha_{crit} = 1.0$ (note that the JETTO definition for the α_{crit} differs from the usual one, as reported in section 2) is used in JINTRAC to match the pedestal predicted by METIS scaling laws. The assumed value of $Z_{eff} = 1.8$ is compatible with the boundary conditions for density and temperature and the sputtering rates computed by COREDIV simulations [57].

The starting point for the JINTRAC modelling is a METIS-BgB simulation of the OP2 baseline scenario at 4.6 MA/2.28 T and $P_{aux} = 17.5$ MW, considering the machine's availability in the initial research phase of JT-60SA. Unlike the OP2 hybrid scenario (section 3), this scenario is not scaled down in terms of current, field, or power.

In JINTRAC, the waveforms for I_p, $< n_e >_{line}$, and P_{aux} are set to match those from METIS. The BgB transport model is used to predict the time evolution of the current density (J_z), main ion density (n_D), electron and ion temperatures (T_e, T_i), and toroidal rotation (Ω). The current ramp-up rate is 0.3 MA s^{-1}, consistent with experimental values for similar-sized tokamaks (JET, JT-60U). The Kadomstev model [59] is implemented in JINTRAC to simulate sawteeth effects in the plasma core, with a fixed crash timing of 200 ms.

Figures 21 and 22 compare the time traces and plasma kinetic profiles from JINTRAC-BgB and METIS-BgB simulations of the OP2 baseline scenario. Most differences between the two codes arise from variations in the density profile and power deposition profile. METIS (with a prescribed n_e profile)

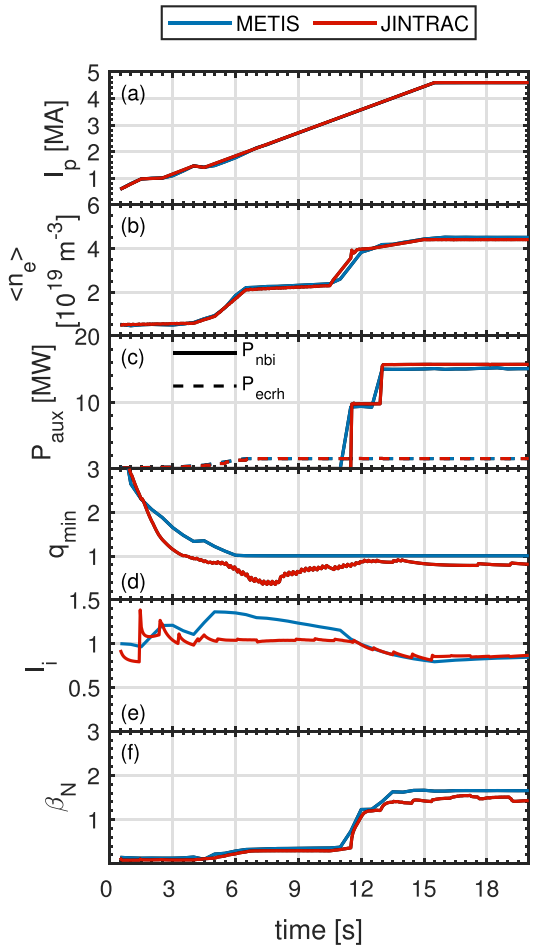

Figure 21. Time evolution of the plasma current (I_p), line averaged electron density ($< n_e >_{line}$), NBI end ECRH powers (P_{nbi}, P_{ecrh}), minimum value of the safety factor (q_{min}), internal inductance (l_i) and normalised beta (β_N) computed by the 0.5-D code METIS (blue) and the 1.5-D code JINTRAC (red) for the OP2 baseline scenario.

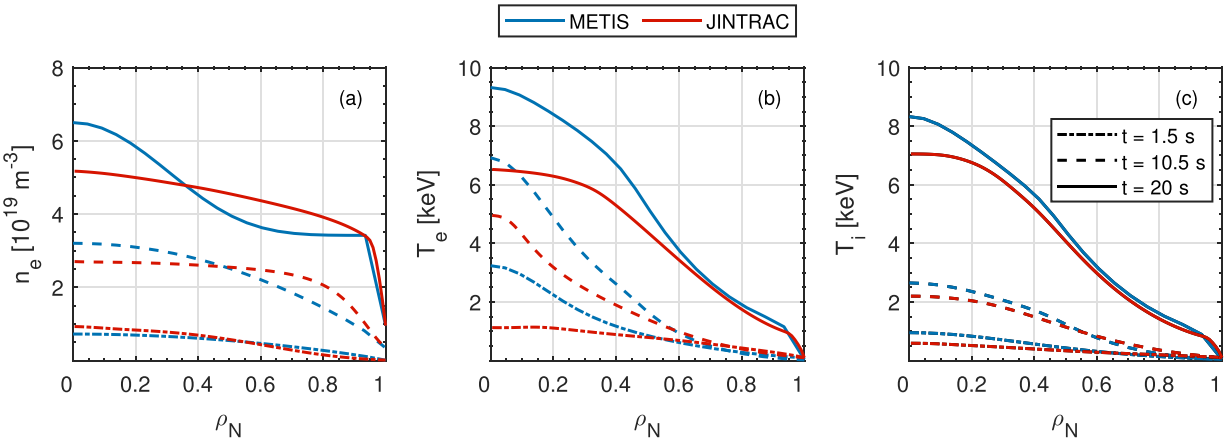

Figure 22. Profiles of the electron density (n_e), electron temperature (T_e) and ion temperature (T_i) computed by JINTRAC (red) and METIS (blue) for the OP2 baseline scenario. The quantities are shown at three different time of the simulation: at the beginning of the ramp-up phase (1.5 s), when the initial conditions had enough time to relax; after the ECRH injection and before the switching-on of the NBI (10.5 s); at the end of the simulation and ∼5 s into the flat-top phase (20 s).

shows lower density between $0.5 < \rho_N < 0.95$ compared to JINTRAC-BgB and exhibits a 20% higher density peaking factor. As a result, NBI penetration is deeper in METIS, with most NBI power deposited near the axis (shown in figure 23, box (*c*)), leading to higher T_e and T_i than in JINTRAC. Additionally, sawtooth modelling in JINTRAC keeps the core temperature lower than in METIS by expelling particles and energy during each sawtooth crash.

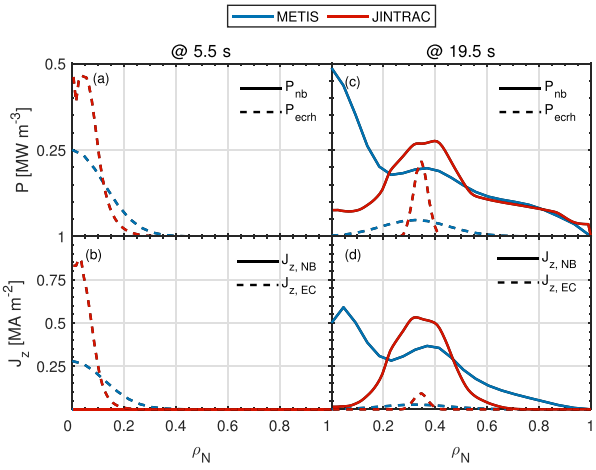

Figure 23. Heating (top) and current drive (bottom) deposition profiles computed by JINTRAC (red) and METIS (blue) for the OP2 baseline scenario. The profiles are shown both during the ramp-up phase (left) and during the flat-top phase (right).

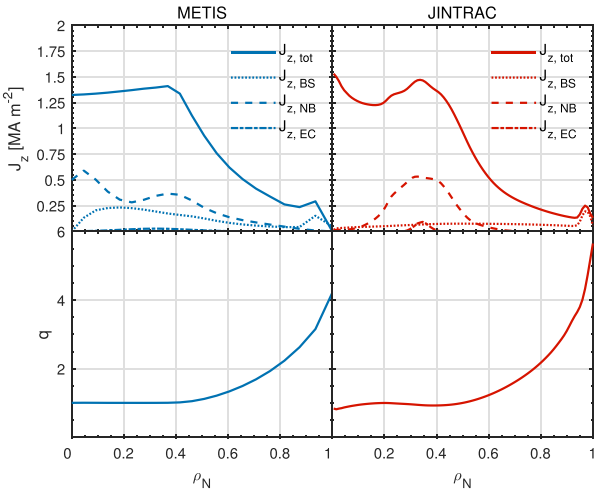

Figure 24. Composition of the current density (J_z) profile (top) and safety factor profile (bottom) for the OP2 baseline scenario during the flat-top phase computed by METIS (left) and JINTRAC (right). The total current density ($J_{z,\mathrm{tot}}$), the bootstrap current density ($J_{z,\mathrm{BS}}$), the NBI current density ($J_{z,\mathrm{NB}}$) and the EC current density ($J_{z,\mathrm{EC}}$) are shown.

In JINTRAC, the $q = 1$ surface appears earlier in the plasma (3.4 s) compared to METIS (6 s), mainly due to the higher on-axis $J_{z,\mathrm{EC}}$ current calculated by GRAY during the ramp-up phase (figure 23, box (*a*)), which lowers q_{min}. To align the centre of the Gaussian deposition profile in METIS, a poloidal injection angle of $\alpha = 35.5°$ is used in GRAY, while a toroidal injection angle of $\beta = 20°$ is used to match the EC current fraction $I_{\mathrm{ECCD}}/I_{\mathrm{p}}$. As the centre of the EC profile shifts from $\rho_{\mathrm{N}} = 0$ to $\rho_{\mathrm{N}} = 0.35$ from ramp-up to the flat-top phase, a $-20°$ shift in α is applied. Similarly to the OP2 hybrid scenario (section 3), the EC power and current profiles computed by GRAY are narrower and exhibit higher peaks than those in METIS.

Figure 24 shows the total current density profile, including contributions from the bootstrap current ($J_{z,\mathrm{BS}}$), NBI current ($J_{z,\mathrm{NB}}$), EC current ($J_{z,\mathrm{EC}}$), and the safety factor. The slight hollowness of the JINTRAC current profile results from the overlap of $J_{z,\mathrm{NB}}$ and $J_{z,\mathrm{EC}}$ (calculated by PENCIL and GRAY, respectively), both centred around $\rho_{\mathrm{N}} \sim 0.35$, driving a strong off-axis current, with the main contribution from the N-NBI. The bootstrap current between $0 < \rho_{\mathrm{N}} < 0.4$ is lower in JINTRAC due to a reduced pressure gradient in this region compared to METIS, resulting in a bootstrap current fraction of $f_{\mathrm{BS}} \sim 14\%$ during the flat-top phase.

The normalized beta value computed by JINTRAC is $\beta_{\mathrm{N}} = 1.5$, consistent with typical β_{N} values for the baseline scenario at this power level (e.g. see [64]). However, the confinement enhancement factor H_{98} is somewhat lower ($H_{98} = 0.87$) than the expected value of 1.0. Preliminary JT-60SA OP2 pedestal predictions using the EPED1 model [61] suggest that the pedestal height imposed in METIS may be too low. For the same density pedestal height, $T_{\mathrm{e,ped}}$ and $T_{\mathrm{i,ped}}$ values four times higher than those in METIS are predicted. As a result, scanning the α_{crit} value in the ETB of JINTRAC simulations is useful to assess the sensitivity of τ_{E} predictions to pedestal assumptions.

Figure 25 reports the results of the α_{crit} scan in terms of plasma kinetic profiles ($n_{\mathrm{e}}, T_{\mathrm{e}}, T_{\mathrm{i}}$). A $\beta_{\mathrm{N}} = 1.8$ and $H_{98} = 1.07$ is found for $\alpha_{\mathrm{crit}} = 2.0$, while the maximum $\beta_{\mathrm{N}} = 2.7$ and $H_{98} = 1.6$ occurs for $\alpha_{\mathrm{crit}} = 4.0$, when $T_{\mathrm{e,ped}} = 3.8$ keV is reached. The temperature profiles remain stiff, with core values increasing in proportion to the pedestal height while maintaining a constant gradient. This indicates that the improvement in confinement is highly dependent on the confinement conditions in the pedestal, which are controlled by the choice of the α_{crit} value.

5. Discussion

The integrated modelling of two plasma scenarios proposed for Operational Phase 2 (OP2) of JT-60SA-namely, the hybrid scenario and the baseline scenario-has been detailed in the preceding sections. The simulations were conducted using the JINTRAC suite of codes, equipped with the BgB semi-empirical transport model employed to simulate the plasma evolution, starting from the ramp-up phase and extending through the initial seconds of the flat-top phase.

Two versions of the OP2 hybrid scenario (3.7 MA/2.28 T and 2.7 MA/1.70 T) are derived from METIS simulations of the Advanced Inductive (hybrid) scenario, following a scaled reduction of plasma current, magnetic field, density, and heating power, followed by an optimization process. The optimization of the 3.7 MA scenario, relative to the reference case, indicates that a slower current ramp-up during the initial phase (from 0.5 to 6 s) followed by a faster ramp in the second phase (from 6 to 10 s), coupled with earlier NBI injection and a more rapid density increase, is required to achieve a $q_{\mathrm{min}} > 1$ throughout the simulation, while maintaining low shine-through losses. The same optimization approach is valid for

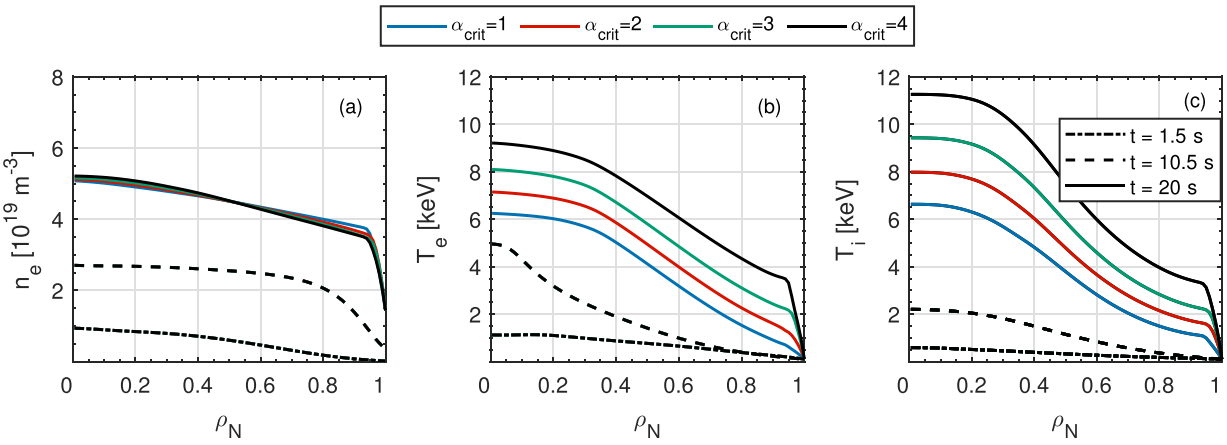

Figure 25. Time evolution of plasma kinetic profiles for different values of the critical normalized pressure gradient $\alpha_{\rm crit}$ in the OP2 baseline scenario at 4.6 MA/2.28 T. (*a*) Electron density profile ($n_{\rm e}$), (*b*) Electron temperature profile ($T_{\rm e}$), and (*c*) Ion temperature profile ($T_{\rm i}$) at different simulation times: 1.5 s, 10.5 s, and 20 s. Results are shown for $\alpha_{\rm crit} = 1$, 2, 3, and 4, highlighting the effect of pedestal assumptions on core plasma profiles.

the 2.7 MA scenario, ensuring that the q profile remains consistently above unity. These scenarios were evaluated for three values of the Greenwald density fraction ($f_{\rm GW} = n_{\rm e}/n_{\rm GW} = 0.8, 0.6$, and 0.4). Results suggest that a hybrid-like q profile can be sustained at $f_{\rm GW} = 0.8$ and 0.6 for the 3.7 MA scenario, and at $f_{\rm GW} = 0.8$ for the 2.7 MA scenario. At lower densities, the scenario becomes over-powered and over-driven due to significant off-axis penetration of Negative-ion-based NBI, resulting in a hollow current density profile and a reversed q profile. A potential solution explored in the modelling involves injecting only half of the N-NBI power from the upper injector unit, which reduces the negative shear region while keeping the q profile above unity. In the 3.7 MA case, even a configuration with 0 MW of N-NBI and 13.5 MW of P-NBI is sufficient to achieve a hybrid-like safety factor profile.

The key plasma parameters for the OP2 hybrid and baseline scenarios are summarized in table 2. $\beta_{\rm N}$ values as high as 3 are achieved at 1.70 T and $f_{\rm GW} = 0.4$ with 19 MW of auxiliary heating, matching the reference $\beta_{\rm N}$ of the Advanced Inductive (hybrid) scenario. This suggests that exploring the high-$\beta_{\rm N}$ regime could be feasible even during the JT-60SA initial research phase. At this power level, the non-inductive current fraction is anticipated to range between 50% and 70%, depending on the plasma density, with the bootstrap current contributing approximately 35%. The enhancement confinement factor, H_{98}, aligns with the reference value of 1.2 at higher densities. As the neutron production rate for the Advanced Inductive (hybrid) scenario calculated by JINTRAC is consistent with the predictions outlined in the JT-60SA Research Plan [1], the values presented in table 2 serve as a preliminary reference for neutron budget estimates in the initial research phase.

The baseline scenario proposed for Operational Phase 2 (OP2) at 4.6 MA/2.28 T ($f_{\rm GW} = 0.4$) has been modelled using JINTRAC-BgB under varying assumptions regarding the critical normalized pressure gradient in the pedestal. This scan was conducted based on preliminary results from the EPED1 code, which suggest that the pedestal predicted by METIS, using scaling laws, may be underestimated for the baseline scenario. Consequently, the predicted H_{98} could exceed the initially anticipated value of 0.9. Specifically, increasing the pedestal temperature at a fixed density leads to a rise in both stored thermal energy and the confinement enhancement factor, as shown in table 2. Furthermore, the core plasma kinetic profiles scale proportionally with the pedestal increase, maintaining a constant gradient in the core region. A confinement factor of $H_{98} = 1.07$ appears achievable at $\alpha_{\rm crit} = 2$, with a $\beta_{\rm N}$ value of 1.8, typical of the baseline scenario, and a stored energy of 10 MJ. The non-inductive current fraction (40%) is lower than that in the hybrid scenario, with a reduced bootstrap current contribution of 18%. Neutron production is generally higher than in the hybrid scenario, a factor that must be considered during scenario development to ensure compliance with neutron budget limitations.

It is evident that an accurate model for predicting both density and temperature is crucial for reliably predicting the performance of a scenario, as the results are highly sensitive to the assumptions made about the pedestal. Future work could verify the pedestal assumptions against the IMEP model [65], developed based on pedestals database of AUG, DIII-D and JET. However, a consistent, physics-based model capable of accurately predicting the H-mode pedestal has yet to be developed, and significant research efforts are being directed toward this goal.

Comparing the flux consumption of the baseline and hybrid scenarios computed by JINTRAC, we observe similar values during the ramp-up phase and a higher value for the baseline scenario after reaching the flat-top phase. This comparison is based on the two reference simulations with similar auxiliary power and temperature pedestal at 40% of the Greenwald fraction, which corresponds to a higher density in the flat-top phase for the baseline scenario. The flux consumption reaches 10 Vs at 8 s in both cases. By the end of the ramp-up phase, the hybrid scenario reaches 10.7 Vs at 10 s, while the baseline scenario reaches 16 Vs at 15 s. The higher flux consumption of the baseline scenario is in line with the higher plasma current achieved (4.6 MA) and the lower non-inductive current

Table 2. Summary of key plasma parameters for the OP2 hybrid and baseline scenarios of JT-60SA. Results are provided for various combinations of plasma current, field, Greenwald fraction and heating, highlighting the differences between the hybrid and baseline scenarios under different operating conditions.

	OP2 hybrid scenario						OP2 baseline scenario				
	3.7 MA/2.28 T			2.7 MA/1.70 T			4.6 MA/2.28 T, $n_e/n_{GW} = 0.4$				
	$n_e/n_{GW} = 0.8$	$n_e/n_{GW} = 0.6$	$n_e/n_{GW} = 0.4$	$n_e/n_{GW} = 0.8$	$n_e/n_{GW} = 0.6$	$n_e/n_{GW} = 0.4$	$\alpha_{crit} = 1$	$\alpha_{crit} = 2$	$\alpha_{crit} = 3$	$\alpha_{crit} = 4$	METIS
Main ion	D	D	D	D	D	D	D	D	D	D	D
B_t (T)	2.28	2.28	2.28	1.70	1.70	1.70	2.28	2.28	2.28	2.28	2.28
I_p (MA)	3.70	3.70	3.70	2.70	2.70	2.70	4.60	4.60	4.60	4.60	4.60
f_{bs} (%)	27.24	30.56	37.26	32.22	33.62	36.73	14.27	17.95	23.62	31.04	17.15
f_{ni} (%)	35.99	49.04	60.03	51.70	48.86	70.81	34.35	40.55	49.08	59.51	41.33
f_{gw} (%)	79.45	59.67	40.25	79.05	60.58	40.96	41.92	41.93	41.95	41.95	43.00
q_{95}	3.99	4.05	4.10	4.13	4.14	4.28	3.61	3.75	3.92	4.25	3.32
$P_{N\text{-}NBI}, P_{P\text{-}NBI}$ (MW)	10,6	10,6	5 (U), 11	10, 6	5 (U), 11	5 (U), 11	10, 6	10, 6	10, 6	10, 6	10, 6
P_{ecrh} (MW)	1.50 × 100 s, 1.50 × 5 s	1.50 × 100 s, 1.50 × 5 s	1.50 × 100 s, 1.50 × 5 s	1.50 × 100 s, 1.50 × 5 s	1.50 × 100 s, 1.50 × 5 s	1.50 × 100 s, 1.50 × 5 s	1.50	1.50	1.50	1.50	1.50
$P_{Shine\text{-}Through}$ (MW)	0.12	0.13	0.44	0.15	0.29	0.90	0.29	0.31	0.32	0.33	0.94
P_{rad} (MW)	2.11	1.73	1.40	1.55	1.35	1.18	0.62	0.65	0.70	0.76	1.14
$n_{e,0}, < n >$	8.15, 7.19,	6.33, 5.40,	5.09, 3.64,	5.86, 5.22,	4.91, 4.00,	3.59, 2.70,	5.17, 4.40,	5.14, 4.40,	5.20, 4.40,	5.26, 4.40,	6.48, 4.50,
$, n_{e,ped} (10^{19}$ m$^{-3})$	5.20	3.39	1.86	4.15	2.70	1.62	3.38	3.60	3.47	3.43	3.43
$T_{e,0}, < T_e >, T_{e,ped}$	4.66, 2.68,	6.54, 3.74,	9.67, 6.20,	4.61, 2.43,	5.57, 2.95.	7.26, 4.16,	6.70, 3.23,	7.45, 3.83,	8.45, 4.74,	9.61, 5.93,	9.44, 3.71,
(keV)	1.35	2.10	4.55	1.06	1.44	2.45	1.08	1.56	2.46	3.80	1.15
$T_{i,0}, < T_i >, T_{i,ped}$	4.66, 2.51,	6.62, 3.44,	13.63, 6.44,	4.54, 2.22,	6.34, 2.95,	10.54, 4.81,	7.32, 3.04,	8.46, 3,95,	10.02, 4.89,	11.98, 6.18,	8.48, 3.16,
(keV)	1.18	1.61	3.01	0.97	1.31	2.15	0.91	1.90	2.39	3.26	0.89
W_{th} (MJ)	10.20	10.62	12.07	6.68	6.42	6.49	8.41	10.25	12.57	15.71	9.10
β_n, β_p	2.04, 0.91	2.28, 1.05	2.72, 1.17	2.66, 1.11	2.63, 1.13	3.06, 1.29	1.49, 0.42	1.8, 0.54	2.2, 0.71	2.72, 0.93	1.65, 0.54
τ_E (S)	0.65	0.51	0.45	0.36	0.32	0.42	0.49	0.60	0.74	0.93	0.53
H_{98}	1.12	1.30	1.76	1.16	1.25	1.50	0.87	1.07	1.31	1.64	1.00
Z_{eff}	2.10	2.10	2.10	2.10	2.10	2.10	1.80	1.80	1.80	1.80	1.80
neutrons $(10^{16}$ s$^{-1})$	2.62	4.41	5.58	2.43	1.89	2.94	4.32	5.33	6.96	9.32	5.67

fraction (50%) with respect to the hybrid scenario (2.7 MA, $f_{ni} = 71\%$).

Furthermore, the resistive flux consumption is 2.5 to 3 times higher in the hybrid scenario due to its lower electron temperature and higher resistivity compared to the baseline. This difference arises primarily for two reasons, both leading to higher $T_{e,0}$ in the baseline case: (i) the EC power during the ramp-up phase is deposited on-axis in the baseline scenario (see figure 23), and (ii) the density is increased more slowly compared to the hybrid scenario. As a result, despite the lower EC power in the baseline scenario, the electron temperature remains consistently higher throughout the ramp-up phase, leading to lower resistivity and lower resistive flux consumption.

6. Conclusions

The integrated modelling of two plasma scenarios—hybrid and baseline—proposed for the second operational phase (OP2) of JT-60SA was performed using the JINTRAC suite of codes, equipped with the BgB transport model. These simulations, covering the ramp-up phase through the initial seconds of the flat-top phase, offer valuable insights into the feasibility of achieving the target plasma parameters and provide a foundation for further physics studies within the JT-60SA Experiment Team (e.g. MHD stability, gyrokinetic analyses, plasma control).

The hybrid scenario was modelled at both 3.7 MA/2.28 T and 2.7 MA/1.70 T with $P_{aux} = 19$ MW by scaling down the plasma current, magnetic field, density, and power from the reference METIS simulation at 3.5 MA/2.28 T and $P_{aux} = 37$ MW. JINTRAC predictions closely aligned with the METIS results, showing differences in the main plasma parameters within 10%. Optimization of the ramp-up phase was necessary to produce a q profile above one with a low magnetic shear region. The optimization indicated that a slower current ramp-up in the initial phase (0.5 to 6 s) followed by a faster ramp in the second phase (from 6 to 10 s), combined with earlier NBI injection and a more rapid density increase, was required to maintain $q_{min} > 1$ throughout the simulation while minimizing shine-through losses. Results for the OP2 hybrid scenario at 2.7 MA showed that β_N values around 3 and high non-inductive current fractions (50%–70%) can be achieved at $P_{aux} = 19$ MW ($P_{N-NBI} = 5$ MW from the upper injector, $P_{P-NBI} = 11$ MW, $P_{ECRH} = 3$ MW). Adjusting the N-NBI power to 5 MW from the upper unit, rather than 10 MW from both units, effectively prevented hollow current density and reversed q profiles, ensuring that $q_{min} > 1$ was maintained. This high-β_N regime envisioned for the OP2 hybrid scenario, characteristic of the Advanced Inductive (hybrid) scenario planned for the Extended Research Phase, offers an early opportunity to study MHD stability limits during the initial research phase.

The baseline scenario for OP2 at 4.6 MA/2.28 T was modelled under varying assumptions about the pedestal pressure gradient. Preliminary results from the EPED1 model suggest that METIS may underestimate the pedestal height. Consequently, confinement enhancement factors (H_{98}) higher than those predicted for lower pedestal heights are possible. A confinement factor of $H_{98} = 1.07$ appears achievable with $\alpha_{crit} = 2$, corresponding to a β_N value of 1.8, typical of the baseline scenario, and a stored energy of $\sim$10 MJ.

Accurate modelling of density and temperature profiles is crucial for achieving reliable plasma performance predictions, as the results are highly sensitive to pedestal assumptions. Developing a robust, physics-based model for predicting the H-mode pedestal remains an ongoing challenge and will require further research efforts.

Future work will prioritize the use of first-principle models such as QuaLiKiz and TGLF, which offer a more accurate representation of turbulent transport processes, and of the semi-empirical CDBM transport model. To ensure robust scenario development, the controllability of the plasma will be carefully evaluated through dedicated control codes like CREATE-NL and MECS. The modelling of the NBI system can be improved by employing the Monte Carlo code ASCOT, which allows for a more precise simulation of fast ion behaviour and beam deposition profiles. Furthermore, a thorough analysis of the stability properties of the pedestal profiles will be essential. This can be achieved by using state-of-the-art stability codes, like MISHKA.

Acknowledgments

This work has been carried out within the framework of the EUROfusion Consortium, funded by the European Union via the Euratom Research and Training Programme (Grant Agreement No. 101052200—EUROfusion). Views and opinions expressed are however those of the author(s) only and do not necessarily reflect those of the European Union or the European Commission. Neither the European Union nor the European Commission can be held responsible for them.

JT-60SA was jointly constructed and is jointly funded and exploited under the Broader Approach Agreement between Japan and EURATOM.

ORCID iDs

S. Gabriellini https://orcid.org/0000-0001-9488-5193
V.K. Zotta https://orcid.org/0000-0002-3518-5178
L. Garzotti https://orcid.org/0000-0002-3796-9814
N. Aiba https://orcid.org/0000-0002-0652-2892
G. Pucella https://orcid.org/0000-0002-9923-2770
C. Sozzi https://orcid.org/0000-0001-8951-0071
D. Taylor https://orcid.org/0000-0002-0465-2466
T. Wakatsuki https://orcid.org/0000-0002-4707-4547

References

[1] 2018 JT-60SA research plan, version 4.0
[2] Giruzzi G. *et al* 2020 *Plasma Phys. Control. Fusion* **62** 014009
[3] Shirai H. *et al* 2024 *Nucl. Fusion* **64** 112008
[4] Yoshida M. *et al* 2024 Start-up of plasma operation and control in the large superconducting tokamak JT-60SA *50th*

EPS Conf. on Plasma Physiscs (*Salamanca, Spain*, *8–12 July 2024*) [I.265]
[5] Inoue S. *et al* 2024 Equilibrium control in the integrated commissioning of JT-60SA *50th EPS Conf. on Plasma Physiscs* (*Salamanca, Spain*, *8–12 July 2024*) [P5.072] (available at: https://lac913.epfl.ch/epsppd2/2024/html/PDF/P5-072.pdf)
[6] Ohtani Y. *et al* 2024 Performance of JT-60SA plasma in the first plasma operation phase *50th EPS Conf. on Plasma Physiscs* (*Salamanca, Spain*, *8–12 July 2024*) [P5.066] (available at: https://lac913.epfl.ch/epsppd2/2024/html/PDF/P5-066.pdf)
[7] Szepesi T. *et al* 2024 Analysis of the first plasmas of JT-60SA using EDICAM video diagnostic *50th EPS Conf. on Plasma Physiscs* (*Salamanca, Spain*, *8–12 July 2024*) [P5.080] (available at: https://lac913.epfl.ch/epsppd2/2024/html/PDF/P5-080.pdf)
[8] Kojima S. *et al* 2024 Validation of plasma equilibrium flight simulator: MECS code in JT-60SA *50th EPS Conf. on Plasma Physiscs* (*Salamanca, Spain*, *8–12 July 2024*) [P4.108] (available at: https://lac913.epfl.ch/epsppd2/2024/html/PDF/P4-108.pdf)
[9] Yokoyama T. *et al* 2024 Disruptions observed in the first plasma operation phase of JT-60SA *50th EPS Conf. on Plasma Physiscs* (*Salamanca, Spain*, *8–12 July 2024*) [P5.057] (available at: https://lac913.epfl.ch/epsppd2/2024/html/PDF/P5-057.pdf)
[10] Hayashi T., Takechi M., Matsunaga G. and Isayama A. 2021 *Fusion Eng. Des.* **170** 112677
[11] Hayashi T. , Matsunaga G., Takechi M. and Isayama A. 2023 *Fusion Eng. Des.* **194** 113666
[12] Hayashi T. *et al* 2023 Completion of the First Lower Divertor Cassette of JT-60SA *15th Int. Symp. Fusion Nuclear Technology (ISFNT-15)* (*Las Palmas de Gran Canaria, Spain*, *10–15 Septembe 2023*) (available at: https://isfnt2023.com)
[13] Tani K., Azumi N. and Devoto R.S. 1992 *J. Comput. Phys.* **98** 332
[14] Artaud J.F. *et al* 2018 *Nucl. Fusion* **58** 105001
[15] Giruzzi G. *et al* 2012 Integrated modelling of JT-60SA scenarios with the METIS code *39th EPS Plasma Physics Conf. - 16th Int. Congress on Plasma Physics* (*Stockholm, Sweden*, *2–6 July 2012*) [P5.018] (available at: https://info.fusion.ciemat.es/OCS/EPSICPP2012PAP/pdf/P5.018.pdf)
[16] Romanelli M. (EFDA-JET Contributors) 2014 *Plasma Fusion Res.* **9** 3403023
[17] Pereverzev G.V. and Yushmanov P.N. 2002 ASTRA automated system for transport analysis in a tokamak IPP-Report 5/98 (Max-Planck-Institut fur Plasmaphysik) (available at: www2.ipp.mpg.de/git/astra/astra.pdf)
[18] Artaud J.F. *et al* 2010 *Nucl. Fusion* **50** 043001
[19] Hayashi N. (JT-60 Team) 2010 *Phys. Plasmas* **17** 056112
[20] Waltz R.E., Staebler G.M., Dorland W., Hammett G.W., Kotschenreuther K. and Konings J.A. 1997 *Phys. Plasmas* **4** 2482
[21] Itoh K., Itoh S.-I., Fukuyama A., Yagi M. and Azumi M. 1994 *Plasma Phys. Control. Fusion* **36** 279
[22] Erba M., Cherubini A., Parail V.V., Springmann E. and Taroni A. 1997 *Plasma Phys. Control. Fusion* **39** 261
[23] Garzotti L. *et al* 2018 *Nucl. Fusion* **58** 026029
[24] Zotta V.K. *et al* 2022 *Nucl. Fusion* **62** 076024
[25] Garcia J. *et al* 2023 *Nucl. Fusion* **63** 112003
[26] Kim H.-T. *et al* 2023 *Nucl. Fusion* **63** 112004
[27] Zotta V.K. *et al* 2022 Predictive modelling of D-T fuel mix control with gas puff and pellets for JET 3.5 MA baseline scenario *48th EPS Conf. on Plasma Physics* (*Maastricht, Netherlands (online)*, *27 June–1 July 2022*) [P2a.115] (available at: https://info.fusion.ciemat.es/OCS/EPS2022PAP/pdf/P2a.115.pdf)
[28] Miyata Y., Suzuki T., Fujita T., Ide S. and Urano H. 2012 *Fusion Res.* **7** 1405137
[29] Miyata Y., Suzuki T., Ide S., Urano H. and Fujita T. 2013 *Plasma Fusion Res.* **8** 2405109
[30] Heumann H. *et al* 2015 *J. Plasma Phys.* **81** 905810301
[31] Ostuni V. *et al* 2021 *Nucl. Fusion* **61** 026021
[32] Morales J. *et al* 2021 *Plasma Phys. Control. Fusion* **63** 025014
[33] Albanese R., Ambrosino R. and Mattei M. 2015 *Eng. Des.* **96-97** 664
[34] van Dongen J., Felici F., Hogeweij G.M.D., Geelen P. and Maljaars E. 2014 *Plasma Phys. Control. Fusion* **56** 125008
[35] Wehner W. , Schuster E., Boyer M.D. and Poli F.M. 2019 *Fusion Eng. Des.* **146** 547–50
[36] Van Mulders S. *et al* 2024 *Nucl. Fusion* **64** 026021
[37] Van Mulders S. *et al* 2021 *Nucl. Fusion* **61** 086019
[38] Parail V. *et al* 2009 *Nucl. Fusion* **49** 075030
[39] Parail V. *et al* 2013 *Nucl. Fusion* **53** 113002
[40] Hogeweij G.M.D. *et al* 2013 *Nucl. Fusion* **53** 013008
[41] Gabriellini S. *et al* 2023 Integrated modelling of the ramp-up phase of the hybrid scenario for the JT-60SA tokamak *49th EPS Conf. on Contr. Fusion and Plasma Phys* (*Bordeaux, France*, *3–7 July 2023*) [P1.062] (available at: https://lac913.epfl.ch/epsppd3/2023/html/Mo/Mo_MCF62_Gabriellini.pdf)
[42] Gabriellini S. *et al* 2024 Integrated modelling of the ramp-up phase of JT-60SA baseline and hybrid scenarios in view of operations *50th EPS Conf. on Contr. Fusion and Plasma Phys* (*Salamanca, Spain*, *8–12 July 2024*) [P5.051] (available at: https://lac913.epfl.ch/epsppd2/2024/html/PDF/P5-051.pdf)
[43] Cennacchi G. and Taroni A. 1988 *JETTO: a free-boundary plasma transport code* ENEA Report RTI/TIB(88)5 (available at: https://inis.iaea.org/records/7h4y6-32977)
[44] Cenacchi G. and Rulli M. 1988 Upgrading of an equilibrium transport code for a multispecies free-boundary plasma *ENEA Report RTI/TIB(88)5*
[45] Garcia J. *et al* 2014 *Nucl. Fusion* **54** 093010
[46] Hayashi N. *et al* 2017 *Nucl. Fusion* **57** 126037
[47] Orsitto F.P. *et al* 2024 High beta experiments on JET in preparation of JT60SA *50th EPS Conf. on Contr. Fusion and Plasma Physics* (*Salamanca, Spain*, *8–12 July 2024*) [P1.051] (available at: https://lac913.epfl.ch/epsppd3/2024/html/PDF/P1-051.pdf)
[48] Bourdelle C., Citrin J., Baiocchi B., Casati A., Cottier P., Garbet X. and Imbeaux F. 2016 *Plasma Phys. Control. Fusion* **58** 014036
[49] Citrin J. *et al* 2017 *Plasma Phys. Control. Fusion* **59** 124005
[50] Staebler G.M., Kinsey J.E. and Waltz R.E. 2005 *Phys. Plasmas* **12** 102508
[51] Tamor S. 1981 *J. Comput. Phys.* **40** 104
[52] Challis C.D., Cordey J.G., Hamnén H., Stubberfield P.M., Christiansen J.P., Lazzaro E., Muir D.G., Stork D. and Thompson E. 1989 *Nucl. Fusion* **29** 563
[53] Farina D. 2007 *Fusion Sci. Technol.* **52** 154–60
[54] Martin Y.R. *et al* 2008 *J. Phys.: Conf. Ser.* **123** 012033
[55] McDonald D.C. *et al* 2007 *Nucl. Fusion* **47** 147
[56] Lauro Taroni L. 1994 Impurity transport of high performance dischareges in JET *21st EPS Conf. Controlled Fusion and Plasma Physics ECA* (*Montpellier, France*, *27 June–1*

July 1994) p 102 (available at: https://library.ipp.mpg.de/EPS_21_Vol1_1994.pdf)
[57] Zagórski R. *et al* 2016 *Nucl. Fusion* **56** 016018
[58] Houlberg W.A., Shaing K.C., Hirshman S.P. and Zarnstorff M.C. 1997 *Phys. Plasmas* **4** 3230
[59] Kadomstev B.B. 1975 *Sov. J. Plasma Phys.* **1** 389
[60] Eriksson L.-G. *et al* 2006 *Nucl. Fusion* **46** S951
[61] Snyder P.B., Groebner R.J., Leonard A.W., Osborne T.H. and Wilson H.R. 2009 *Phys. Plasmas* **16** 056118
[62] Gabriellini S. *et al* 2023 *Nucl. Fusion* **63** 086025
[63] Zotta V.K. *32nd ITPA Transport and Confinement Group Meeting* (*Cadarache, France*, *16–18 April 2024*)
[64] Garzotti L. *et al* 2019 *Nucl. Fusion* **59** 076037
[65] Luda T. *et al* 2021 *Nucl. Fusion* **61** 126048